2-((1-phenyl-1*H*-1,2,3-triazol-4-yl)methyl)-2-azabicyclo[3.2.1]octan-3-one derivatives: simplification and modification of aconitine scaffold for the discovery of novel anticancer agents

Yi Zhang, Ting-jian Zhang, Xin-yang Li, Jing-wei Liang, Shun Tu, Hai-li Xu, Wen-han Xue, Xin-hua Qian, Zhen-hao Zhang, Xu Zhang, Fan-hao Meng

PII: S0223-5234(20)30960-0

DOI: https://doi.org/10.1016/j.ejmech.2020.112988

Reference: EJMECH 112988

To appear in: *European Journal of Medicinal Chemistry*

Received Date: 6 October 2020

Revised Date: 29 October 2020

Accepted Date: 1 November 2020

Please cite this article as: Y. Zhang, T.-j. Zhang, X.-y. Li, J.-w. Liang, S. Tu, H.-l. Xu, W.-h. Xue, X.-h. Qian, Z.-h. Zhang, X. Zhang, F.-h. Meng, 2-((1-phenyl-1*H*-1,2,3-triazol-4-yl)methyl)-2-azabicyclo[3.2.1]octan-3-one derivatives: simplification and modification of aconitine scaffold for the discovery of novel anticancer agents, *European Journal of Medicinal Chemistry*, https://doi.org/10.1016/j.ejmech.2020.112988.

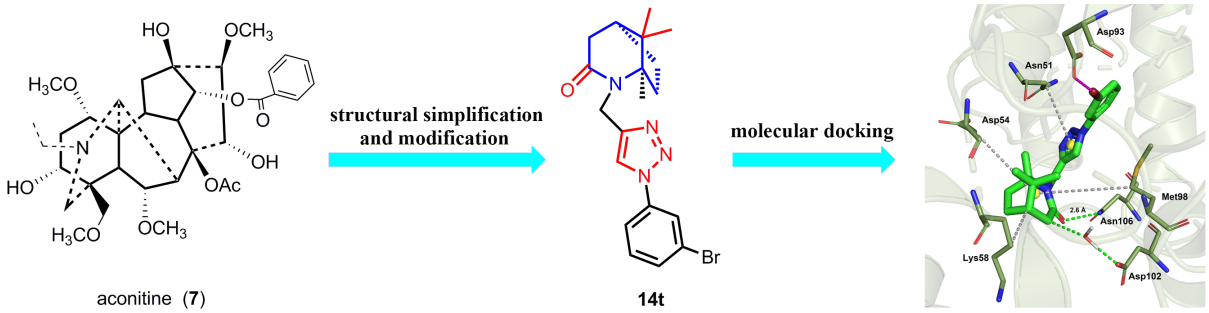

aconitine (**7**)

14t

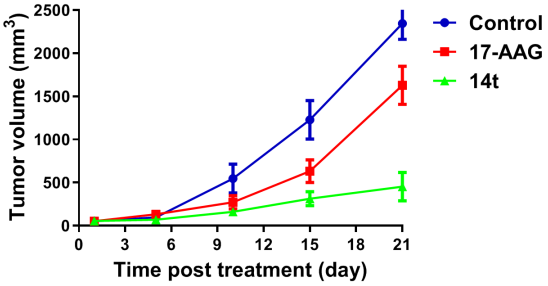

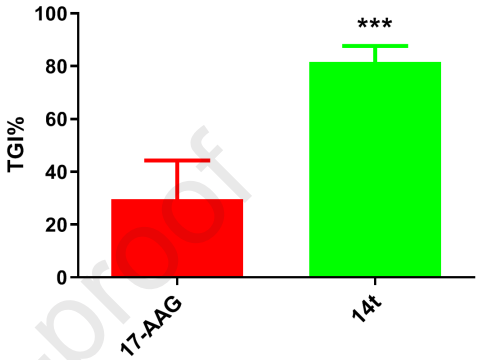

2-((1-phenyl-1*H*-1,2,3-triazol-4-yl)methyl)-2-azabicyclo[3.2.1]octan-3-one derivatives: simplification and modification of aconitine scaffold for the discovery of novel anticancer agents

Yi Zhang [a, 1], Ting-jian Zhang [a, 1], Xin-yang Li [a, b], Jing-wei Liang [a], Shun Tu [a], Hai-li Xu [a], Wen-han Xue [a], Xin-hua Qian [a], Zhen-hao Zhang [a], Xu Zhang [a], Fan-hao Meng [a, *]

[a] School of Pharmacy, China Medical University, 77 Puhe Road, North New Area, Shenyang, 110122, China

[b] Department of Pharmacy, Shengjing Hospital of China Medical University, Shenyang 110122, China

[1] These two authors contributed equally to this work

* Corresponding author: Professor Fan-hao Meng

E-mail address: fhmeng@cmu.edu.cn (F. H. Meng)

Fax: +86-24-31939448

Abstract

The molecular chaperone heat shock protein 90 (Hsp90) is a promising target for cancer therapy. Natural product aconitine is a potential Hsp90 inhibitor reported in our previous work. In this study, we designed and synthesized a series of 2-((1-phenyl-1*H*-1,2,3-triazol-4-yl)methyl)-2-azabicyclo[3.2.1]octan-3-one derivatives as potent Hsp90 inhibitors by simplifying and modifying aconitine scaffold. Among these compounds, **14t** exhibited an excellent antiproliferative activity against LoVo cells with an IC_{50} value of 0.02 μM and a significant Hsp90α inhibitory activity with an IC_{50} value of 0.71 nM. Molecular docking studies provided a rational binding model of **14t** in complex with Hsp90α. The following cell cycle and apoptosis assays revealed that compound **14t** could arrest cell cycle at G1/S phase and induce cell apoptosis via up-regulation of bax and cleaved-caspase 3 protein expressions while inhibiting the expressions of bcl-2. Moreover, **14t** could inhibit cell migration in LoVo and SW620 cell lines. Consistent with *in vitro* results, **14t** significantly repressed tumor growth in the SW620 xenograft mouse model.

Key words: Hsp90 inhibitors; Aconitine; Structural simplification; Antiproliferative activity

1. Introduction

Heat shock protein 90 (Hsp90, 90 kDa) is a ubiquitous molecular chaperone that is responsible for the maturation, stabilization and activation of numerous client proteins related to signal transduction in the cell [1, 2]. Hsp90 regulates more than 500 clients include many oncogenic proteins (*e.g.*, EGFR, c-Met, Src, Akt, c-Raf, Cdk4, MMP2, HIF-1α), which are necessary for the development and progression of cancer [3-9]. Oncogenic mutations of client proteins require increased Hsp90 activity. In fact, Hsp90 is overexpressed in cancer cells 2-10 fold higher than normal cells and exists as activated multi-chaperone complexes in cancer cells [10]. Therefore, inhibition of the molecular chaperone Hsp90 represents a promising chemotherapeutic strategy toward the treatment of various types of cancers [2, 11-13].

In humans, Hsp90 exists as four isoforms: Hsp90α, Hsp90β, glucose-regulated protein 94 kDa (Grp94), and tumor necrosis receptor-associated protein 1 (Trap1) [14]. Hsp90α and Hsp90β are localized to the cytoplasm, whereas Grp94 resides in the endoplasmic reticulum, and Trap1 is localized within the mitochondria [15]. Most Hsp90 inhibitors are pan-inhibitors that target both cytosolic isoforms (Hsp90α and Hsp90β) [16]. Hsp90 predominantly exists as a homodimer and is composed of three principal domains: the N-terminal ATP-binding domain, the middle domain and the C-terminal dimerization domain [9, 17]. Over the past decades, a substantial number of Hsp90 inhibitors have been developed, including N-terminal inhibitors and C-terminal inhibitors. Most Hsp90 inhibitors, such as geldanamycin (**1**) [18], SNX-5422 (**2**) [19], radicicol (**3**) [20] and 17-allylamino-17-demethoxygeldanamycin (17-AAG, **4**) [21] are known to interact with the ATP-binding pocket in the N-terminal domain of Hsp90, whereas KU-174 (**5**) [22] and novobiocin (**6**) [23], have shown effective inhibitory activity by interacting with the ATP-binding pocket in the C-terminal domain of Hsp90 (**Fig. 1**). However, none of the Hsp90 inhibitors have been approved by the U.S. Food and Drug Administration (FDA) for the treatment of cancer, challenges such as concomitant induction of the pro-survival heat shock response, hepatotoxicity and multidrug resistance, have impeded their clinical application [13, 24, 25]. Hence, the discovery of novel Hsp90 inhibitors with better biological activities and fewer side effects is still a demanding task.

Natural products (NPs) have been prominent in the development of new antitumor agents [11, 26]. However, NPs generally have structurally complex frameworks and high molecular weights,

leading to synthetic difficulty, unfavorable pharmacokinetic profiles, and poor drug-likeness [26]. Therefore, simplifying complex structures of NPs, while retaining the desired biological activity, is a valid and meaningful strategy in drug development process. This strategy has been successfully used in the lead optimization of NPs and yielded a number of marketed drugs and drug candidates [27-29]. A classic example of the structural simplification of NPs is the development of simplified morphine-derived analgesics (*e.g.*, butophanol, pentazocine, pethidine and methadone), in which the complex pentacyclic system of morphine was simplified via the removal of unnecessary fragments [30].

Aconitine (**7**), a diterpenoid alkaloid isolated from the Chinese plants of Aconitum genera (Ranunculaceae family), has been reported to show effective anticancer properties such as interfering with the cell cycle, inducing apoptosis, and altering multidrug resistance [31, 32]. Our previous investigation indicated the potential for aconitum alkaloids as Hsp90 inhibitor for cancer treatment [33]. However, the structural complexity and natural scarcity hampered the possibility of its clinical application [34, 35]. Thus, the research for more available aconitine analogs with concise framework could be a meaningful work. As shown in **Fig. 2**, most aconitum alkaloids share the general structures and ring numbering systems. Previous structure-activity relationship (SAR) studies have indicated that A-E-F ring framework is essential to biological activity of aconitine-type natural products [34]. Additionally, our team recently illustrated the structure-toxicity relationship (STR) of aconitum alkaloids, and revealed that hydrophilic groups substituted at C2 and C3 (ring A), C8 and C15 (ring C) may be related to neurological toxicities [36]. Analogously, the ester substituents at C14 (ring B) and C8 (ring D) could cause cardio problems according to Nyirimigabo's reports [37]. To this end, our design strategy thus focuses on retaining the E-F ring framework that simplified as a 2-azabicyclo[3.2.1]octane. In addition, the C1 and C10 methyl group are highly conserved and carbonyl group at C19 plays crucial roles in biological functions [38], which thus maintained in our design. Based on the deep understanding of the crystallographic structure of Hsp90 (PDB ID: 2XJX), fragment-based drug design strategy was carried out with 2-azabicyclo[3.2.1]octan-3-one as a core moiety. Using fragment growing method, a lipophilic phenyl moiety was introduced into the molecule, which was connected to the N18 atom of 2-azabicyclo[3.2.1]octan-3-one core through a 1,2,3-triazole. Continuing our previous work [39], we reported herein the design and synthesis of a series of

2-((1-phenyl-1*H*-1,2,3-triazol-4-yl)methyl)-2-azabicyclo[3.2.1]octan-3-one derivatives (**14a-v**) as potent anticancer agents. In addition to the cellular and enzymatic activities evaluations, the molecular docking study was carried out. Moreover, cell cycle arrest, apoptosis and cell migration were investigated and we further biologically evaluated anticancer effects through a xenograft mouse model.

2. Results and discussion

2.1. Chemistry

The synthetic route of 2-((1-phenyl-1*H*-1,2,3-triazol-4-yl)methyl)-2-azabicyclo[3.2.1]octan-3-one derivatives (**14a-v**) is shown in **Scheme 1**. Commercially available (1*S*)-(–)-camphor (**8**) was treated with hydroxylamine to give oxime **9** according to the synthetic protocol described by Kotsikorou [40]. In this procedure, compound **10**, as a key intermediate, was produced from the Beckmann rearrangement of (1*S*)-(–)-camphor oxime (**9**). Briefly, (1*S*)-(–)-camphor oxime (**9)** was activated with methanesulfonyl chloride to produce sulfonate intermediate, then Beckmann rearrangement proceeded via the departure of the sulfonate group and migration of the antiperiplanar carbon to the nitrogen, and tautomerized to camphor lactam **10** [41]. Camphor lactam **10** shared the same stereo configuration with the corresponding moiety of aconitine. Compound **11** was synthesized from the camphor lactam **10** by the action of sodium hydride in dry THF followed by addition of the propargyl bromide. The preparation of various substitute azido benzenes **13a-v** was performed via diazo-reaction and displacement reaction with sodium azide. The 1,3-dipolar cycloaddition of compound **11** with various azido benzenes **13a-v** was subsequently carried out in the presence of copper (II) sulfate and ascorbic acid to give target compounds **14a-v**.

2.2. Biological evaluation

2.2.1. In vitro cytotoxicity assay and heat shock protein 90 inhibition

In this study, MTT assay was used as a preliminary screen for evaluation of *in vitro* cytotoxicity. The antiproliferative effect of all target compounds (**14a-v**) was evaluated against six cancer cell lines: A549, OVCAR-3, HepG2, LoVo, PANC-1 and SGC7901. The results were expressed as IC_{50} values and summarized in **Table 1**, and 17-AAG (**4**), a typical Hsp90 N-terminal

inhibitor, was used as a reference compound.

As shown in **Table 1**, most of the newly synthesized 2-((1-phenyl-1*H*-1,2,3-triazol-4-yl)methyl)-2-azabicyclo[3.2.1]octan-3-one derivatives presented excellent potency against all six cancer cell lines than 17-AAG, revealing that our designed skeleton was greatly beneficial to inhibit tumor cell growth. In addition, all target compounds, except compounds **14a-c**, **14p** and **14r**, had better antiproliferative ability against LoVo cells compared to other five cancer cell lines. Among these compounds, **14j**, **14l**, **14m**, **14p**, **14q**, **14t** and **14v** showed robust activity against A549, OVCAR-3, HepG2 and LoVo cells. Most importantly, compound **14t** showed potent activities against six cancer cell lines with IC_{50} values from 0.02 μM to 0.12 μM, and displayed the best activity against LoVo cells with an IC_{50} value of 0.02 μM. Compound **14q** also exhibited strong antiproliferative activity against A549, OVCAR-3, HepG2 and LoVo cells, with IC_{50} values of 0.06 μM, 0.05 μM, 0.06 μM and 0.07 μM, respectively.

The structure-activity relationship (SAR) studies revealed that the halogen substituents were advantageous to anticancer activities. From the results, it seemed that the *meta*-derivatives usually possessed higher potency in LoVo cell line than its *ortho*- and *para*-derivatives when R group was a halogen (*e.g.*, **14q** versus **14p**, **14r**; **14t** versus **14s**, **14u**). For the *meta*-derivatives, when R = F (**14n**), Cl (**14q**) or Br (**14t**), the antiproliferative activity of compounds was better than the other groups (*e.g.*, **14b**, **14e**, **14h** and **14k**). Particularly, the antiproliferative activity of the bromo analogs (**14s**, **14t** and **14u**) were superior to the chloro analogs (**14p**, **14q** and **14r**) and the fluoro analogs (**14m**, **14n** and **14o**) in LoVo cell line. Correspondingly, compound **14t** with R group substituted by a bromo at the *meta*-position presented excellent anticancer activities.

On the basis of antiproliferative activity, inhibitory effects of compounds **14j**, **14l**, **14m**, **14p**, **14q**, **14t** and **14v** were tested against six normal cell lines: MRC-5, IOSE80, LO2, NCM460, HPDE6-c7 and GSE-1 to evaluate their toxicity and safety. The results were expressed as CC_{50} values and recorded in **Table 2**. Selectivity index (SI) of the drug represents a safe range for evaluating and judging drug effects [42]. The SI value of the compound was obtained by dividing CC_{50} value of the compound against the normal cell, by IC_{50} value of this compound against the corresponding cancer cell line (**Fig. 3**). The larger the index is, the more extensive the safety

ranges. It can be seen from the **Fig. 3**, seven candidate compounds showed high drug selectivity toward liver and colon cancer cell lines. Moreover, compound **14t** was the most selective, showing SI values in the range of 82−527 toward the six cancer cell lines. Besides, *in vitro* human Hsp90α inhibitory activity studies were performed on seven compounds and the results were summarized in **Table 3**. From the results, compounds **14j**, **14m**, **14p**, **14q** and **14t** show significant improvement in Hsp90α inhibitory potency compared to 17-AAG. Especially, compound **14t** exhibited the best Hsp90α inhibition (IC_{50} = 0.71 nM) among the tested compounds. This result was consistent with MTT assays.

In summary, our results indicated that most of the target compounds had excellent antiproliferative ability against LoVo cells compared to other five cancer cell lines, and the introduction of halogens was superior to the other groups. Based on selectivity index, seven candidate compounds displayed the highest drug selectivity for liver and colon cancer cell lines. Among these compounds, **14t** had stronger ability to inhibit both cell viability and Hsp90α enzyme activity than 17-AAG and had more potential of medicinal research significance on the discovery of novel Hsp90 inhibitors. With the above consideration, our study mainly focused on the inhibitory effects of compound **14t** on colon cancer cell lines.

2.2.2. Molecular docking study

In order to identify the interactions of compound **14t** with the amino acid residues of Hsp90, docking studies were performed using Molecular Operating Environment software (MOE, Version 2015.10). The target protein Hsp90α (PDB ID: 2XJX, Resolution 1.66 Å) was retrieved from Protein Data Bank (PDB) and used for docking simulation. As illustrated in **Fig. 4**, compound **14t** occupied a deep ATP-binding pocket of Hsp90α, the O atom of lactam group accepted an H-bond from the Asn106 and H-bond distance was 2.6 Å, and hydrogen bonding energy component contributed −1.5 kcal/mol to the binding. The azabicyclo group linked to the amino acid residue Asp102 via a water bridge. Moreover, the (1*S*,5*S*)-1,8,8-trimethyl-2-azabicyclo[3.2.1]octan-3-one moiety formed hydrophobic interactions with residues Met98, Lys58 and Asp54. In addition, docking study identified a key hydrophobic interaction between the 1,2,3-triazole moiety and Asn51. Interestingly, bromine atom formed a crucial halogen bond with carboxyl group of Asp93, which contributed −5.9 kcal/mol to the binding.

2.2.3. Cell cycle assay

Colon cancer is one of the most common malignancies in the world, approximately 90% of colon cancer deaths arise from cancer metastasis [43, 44]. To investigate the mechanism of cellular cytotoxicity, high metastatic LoVo and SW620 cell lines were treated with different concentrations of compound **14t** (0, 20, 40, and 80 nM) for 24 h. The effects of compound **14t** on cell cycle distribution were determined by flow cytometry analysis using propidium iodide (PI) staining (**Fig. 5A**). The analysis indicated that, as the concentration of the **14t** increased, the cells in the G0/G1 phase increased, and the cells in the G2/M phase decreased. Eventually, compound **14t** induced cycle arrest of LoVo and SW620 cells at the G1/S phase (**Fig. 5B**), suggesting that this might be one of the possible mechanisms for cellular cytotoxicity.

2.2.4. Cell apoptosis assay

Most chemotherapeutic drugs eventually induce apoptosis in cancer cells when they inhibit cell cycle progression, thereby achieving antitumor effects [45]. Therefore, to determine whether the cell cycle arrest caused by the compound **14t** could ultimately induce apoptosis, LoVo and SW620 cells were treated with different concentrations of compound **14t** (0, 20, 40, and 80 nM) for 24 h, then collected and stained with Annexin V-FITC and PI double staining. The apoptotic effects of compound **14t** were determined by flow cytometry analysis. As can be seen from the **Fig. 6A**, the apoptotic rate of LoVo cells was 3.2%, 6.1%, 8.6%, and 32.3% for each concentration respectively. With the increase in concentration, the apoptotic rate increased, of which the late apoptosis rates were 1.6%, 3.1%, 5.4%, and 24.9%. However, the apoptotic rate of SW620 cells was 3.0%, 13.6%, 23.2%, and 49.9% for each concentration respectively. With the increase in concentration, the percentages of apoptotic cell were significantly increased from 3.0% to 49.9% (**Fig. 6B**). The late apoptotic rates of SW620 cells were 1.3%, 8.5%, 15.1%, and 29.3%. These results indicated that compound **14t** could induce apoptosis in the two colon cancer cell lines, and that SW620 cells were more prone to apoptosis than LoVo cells after **14t** treatment.

*2.2.5. The effects on apoptosis-related proteins of **14t**-treated LoVo and SW620 cells*

To elucidate the underlying mechanism of apoptosis induced by **14t**, western blot analysis

was performed to study the expression levels of apoptosis-related proteins. It has been demonstrated that bcl-2 family proteins play a crucial role in regulating the apoptotic pathway, including pro-apoptotic bax and anti-apoptotic bcl-2 proteins [46]. Thus, proteins were treated with **14t** at different concentrations (0, 20, 40 and 80 nM), and the results showed that the levels of bax were markedly increased in the presence of **14t**, whereas levels of bcl-2 were decreased. To further explore the mechanism of apoptosis, we detected the protein expression of cleaved-casepase 3 and caspase 3. As shown in **Fig. 7A**, the activation of caspase-3 caused an increase in cleaved-caspase 3 protein levels, eventually, induced apoptosis.

2.2.6. Cell migration and wound healing assays

Cell migration is a vital possession involved in the dissemination of cancerous cells mostly during cancer metastasis [47]. Herein, we investigated the effects of **14t** on the migration of LoVo and SW620 cells in a transwell assay. From the results, it was clearly observed that **14t** preventing the migration of LoVo and SW620 cells in a dose dependent manner, and the inhibition of SW620 cells migration was more prominent (**Fig. 8A** and **8B**). Wound healing assays also supported the conclusion that **14t** suppressed the migration of LoVo and SW620 cells. The results showed that, comparison of inhibitory effects on the migration of LoVo and SW620 cells with control group, the effects of compound **14t** were significantly different ($P < 0.001$). In addition, the effect was statistically significant after 24 h of incubation at the concentration of 80 nM, in comparison with control cells, keeping the wound nearly intact in SW620 cell monolayers (**Fig. 8B**).

*2.2.7. In vivo antitumor effects of compound **14t***

To evaluate the *in vivo* anti-colon cancer activity of compound **14t**, BABL/c nude mice were inoculated subcutaneously with colonic cancer SW620 cells. After the establishment of solid tumor, two groups of the mice were intraperitoneally treated with 5 mg/kg of 17-AAG and **14t** daily for 21 consecutive days, respectively. There was no significant body weight loss and no obvious adverse effects were observed during the study (**Fig. 9A**), indicating that **14t** has low toxicity in mice. Moreover, it could be seen from **Fig. 9B** and **9C** that in comparison with the vehicle-treated controls, treatment with **14t** at 5 mg/kg significantly inhibited the growth of implanted colon tumors. As depicted in **Fig. 9D**, compound **14t** achieved significant tumor growth

inhibition with tumor growth inhibition (TGI) value of 81.6%. In contrast, 17-AAG failed to exert significant tumor growth inhibition (TGI = 29.6%) as compared with **14t**.

Immunohistochemical labeling of tumor tissue was performed using antibodies for cell proliferation marker (Ki67) and apoptotic cell death (Cleaved-caspase 3). The result was consistent with the above results that the expression of Ki67 in tumors was significantly decreased by treatment with **14t**. Simultaneously, the expression of cleaved-caspase 3 in tumors was significantly increased, and **14t**-treated group exhibited greater efficacy than the 17-AAG-treated and control group (**Fig. 9E**).

3. Conclusion

In this study, in order to find novel Hsp90 inhibitors, a series of 2-((1-phenyl-1*H*-1,2,3-triazol-4-yl)methyl)-2-azabicyclo[3.2.1]octan-3-one derivatives consisting of simplified and modified aconitine scaffold was designed, synthesized and tested for their antiproliferative ability against six cancer cell lines. Among these compounds, **14t** was identified to be the most promising one with excellent antiproliferative effects against LoVo cells (IC_{50} = 0.02 μM) and significant Hsp90α inhibitory activities (IC_{50} = 0.71 nM). Molecular docking studies were employed to support the experimental results and the key interactions were identified. Flow cytometry analysis indicated that compound **14t** could induce cell cycle arrest at the G1/S phase. Additionally, Annexin V-FITC assay and western blot analysis revealed that **14t** inhibited proliferation of cancer cells by inducing apoptosis via up-regulating bax, cleaved-caspase 3, and down-regulating bcl-2 protein expression levels. Consistent with the *in vitro* results, treatment with **14t** effectively suppressed the volumes and size of colon tumors in mice. Overall, our work successfully identified a series of novel Hsp90 inhibitors derived from aconitine through structural simplification and modification. Compound **14t,** as a promising lead, is worthy for the further investigation.

4. Experimental

4.1. Chemistry

All reagents and solvents were purchased from commercial sources and dried prior to use unless noted otherwise. Reactions were monitored by thin-layer chromatography on 0.25 mm

silica gel plates (GF254) and visualized under UV light. Melting points were determined with an electro thermal melting point apparatus, are uncorrected. Optical rotations were measured by WZZ-3 polarimeter in the solvent indicated. ^{1}H NMR and ^{13}C NMR spectra were recorded at 23 °C in $CDCl_3$ on a Bruker spectrometer using TMS as the internal standard. Chemical shifts were reported as δ (ppm) and signal splitting patterns were described as singlet (s), doublet (d), triplet (t), quartet (q), quintet (quint), or multiplet (m), with coupling constants (*J*) in hertz. High-resolution mass spectra (HRMS) were obtained on an electron spray injection (ESI) Bruker micrOTOF-Q mass spectrometer. The purity of the target compounds was confirmed by HPLC analysis performed on Waters BDS C_{18} (200 mm ×4.6 mm, 5 μm) eluting at 1.0 mL/min of methanol and water (50:50 v/v).

*4.1.1. Synthesis of (1S) -(–)-camphor oxime (**9**)*

A solution of (1*S*)-(–)-camphor (**8**) (3.0 g, 19.7 mmol), hydroxylamine hydrochloride (2.1 g, 30.2 mmol) in water (11 mL) was heated at 80 °C under nitrogen. To the stirred suspension was added MeOH (16 mL) followed by a solution of sodium acetate (3.9 g, 47.5 mmol) in water (8 mL). The reaction mixture was heated at reflux under nitrogen for 9 h, the methanol was removed in vacuo, and the aqueous suspension was filtered. The filtered solid was washed with water, recrystallized from 95% EtOH, and dried to get (1*S*)-(–)-camphor oxime (**9**) as a white solid (2.33g, 71% yield). Mp: 117-119 °C. ^{1}H NMR (600 MHz, $CDCl_3$) δ 8.13 (s, 1H), 2.56 (dt, *J* = 17.8, 3.8 Hz, 1H), 2.06 (d, *J* = 17.8 Hz, 1H), 1.93 (t, *J* = 4.4 Hz, 1H), 1.85 (ddd, *J* = 12.4, 8.1, 3.9 Hz, 1H), 1.71 (td, *J* = 12.2, 4.2 Hz, 1H), 1.49 – 1.44 (m, 1H), 1.27 – 1.21 (m, 1H), 1.01 (s, 3H), 0.93 (s, 3H), 0.81 (s, 3H). ^{13}C NMR (150 MHz, $CDCl_3$) δ 169.96, 51.86, 48.35, 43.72, 33.11, 32.75, 27.73, 19.45, 18.64, 11.19.

*4.1.2. Synthesis of (1S,5S)-1,8,8-trimethyl-2-azabicyclo[3.2.1]octan-3-one (**10**)*

To a stirred solution of (1*S*)-(–)-camphor oxime (**9**) (5.38 g, 32.20 mmol) in pyridine (25 mL) at −22 °C, then methanesulfonyl chloride (5.0 mL, 65.10 mmol) was added dropwise. The reaction mixture was stirred at −22 °C for 3 h and then the temperature was raised. After 2 h of additional stirring at room temperature, the mixture was poured onto iced water and extracted with DCM (3 × 50 mL). The combined organic extracts were washed with sodium bicarbonate and brine,

concentrated under reduced pressure. The residue was purified by flash chromatography on silica gel (chloroform-acetone, 3:1) to get camphor lactam **10** as a white solid (0.39 g, 7.2% yield). Mp: 196-197 °C. ^{1}H NMR (600 MHz, $CDCl_3$) δ 6.77 (s, 1H), 2.60 (ddd, J = 18.1, 4.7, 2.5 Hz, 1H), 2.17 (dd, J = 18.1, 1.6 Hz, 1H), 2.08 – 2.01 (m, 1H), 2.01 – 1.96 (m, 1H), 1.95 – 1.88 (m, 2H), 1.54 – 1.47 (m, 1H), 1.13 (s, 3H), 1.02 (s, 3H), 0.97 (s, 3H). ^{13}C NMR (150 MHz, $CDCl_3$) δ 172.69, 63.65, 43.44, 42.84, 40.11, 39.44, 27.77, 23.44, 18.43, 17.95.

*4.1.3. Synthesis of (1S,5S)-1,8,8-trimethyl-2-(prop-2-yn-1-yl)-2-azabicyclo[3.2.1]octan-3-one (**11**)*

To a stirred solution of (1*S*,5*S*)-1,8,8-trimethyl-2-azabicyclo[3.2.1]octan-3-one (**10**) (0.65 g, 3.89 mmol) in dry THF (20 mL) at 0 °C was added NaH (0.11 g, 4.66 mmol). After being stirred for 1 h, propargyl bromide (0.51 g, 4.27 mmol) was added, and then the solution was stirred for 4 h at room temperature. The mixture was quenched with saturated water and extracted with DCM (3 × 20 mL). The combined organic extracts were washed with brine, dried over Na_2SO_4, filtered, and concentrated to give the crude product. The crude product was purified by flash chromatography on silica gel (petroleum ether-EtOAc, 3:1) to get compound **11** as a grey solid (0.33 g, 41% yield). Mp: 183-187 °C. ^{1}H NMR (600 MHz, $CDCl_3$) δ 4.32 (dd, J = 17.7, 2.1 Hz, 1H), 4.01 (dd, J = 17.7, 2.1 Hz, 1H), 3.08 (t, J = 2.4 Hz, 1H), 2.56 – 2.51 (m, 1H), 2.16 – 2.05 (m, 2H), 1.97 (tdd, J = 11.2, 5.7, 3.2 Hz, 1H), 1.85 (t, J = 5.4 Hz, 1H), 1.80 (ddd, J = 13.5, 12.0, 5.2 Hz, 1H), 1.41 – 1.35 (m, 1H), 1.32 (s, 3H), 0.93 (s, 3H), 0.89 (s, 3H). ^{13}C NMR (150 MHz, $CDCl_3$) δ 169.52, 82.14, 73.42, 69.11, 44.69, 42.46, 38.29, 30.42, 28.39, 25.01 (2C), 18.26, 17.02.

*4.1.4. Synthesis of 1-azido-2-hydroxybenzene (**13a**)*

To a solution of 2-hydroxyaniline (**12a**) (1.0 g, 9.16 mmol) in DCM (15 mL) at 0 °C was added concentrated hydrochloride (37%, 1.08 g, 11.0 mmol), followed by a solution of $NaNO_2$ (0.76 g, 11.0 mmol) in 10mL H_2O by consecutive dropwise addition over a period of 10 min with stirring. After stirring for a further 1 h, a solution of NaN_3 (0.77g, 11.91 mmol) in H_2O (5 mL) was added to the above reaction mixture with stirring. The reaction mixture was warm to room temperature and stirred for 4 h. Then the solution was poured into H_2O, extracted with DCM (3 × 20 mL), dried over Na_2SO_4, filtered and concentrated in vacuo to give **13a** as yellow oil (1.20 g,

97% yield), which was used for the next step without further purification.

Compounds **13b-v** were prepared with the same method and the appropriate substituted aniline.

*4.1.5. Synthesis of (1S,5S)-2-((1-(2-hydroxyphenyl)-1H-1,2,3-triazol-4-yl)methyl)-1,8,8-trimethyl-2-azabicyclo[3.2.1]octan-3-one (**14a**)*

To a stirred solution of 1-azido-2-hydroxybenzene (**13a**) (180 mg, 1.65 mmol) in tBuOH (10 mL), the water solution (10 mL) of copper sulfate pentahydrate (37 mg, 0.15 mmol) and ascorbic acid (79 mg, 0.45 mmol) was added, and then (1*S*,5*S*)-1,8,8-trimethyl-2-(prop-2-yn-1-yl) -2-azabicyclo[3.2.1]octan-3-one (**11**) (287 mg, 1.5 mmol) was added. The reaction mixture was stirred at 60 °C for 8 h and then was concentrated in vacuo, diluted with H_2O and extracted with EtOAc (3 × 15 mL). The combined organic phases were dried over anhydrous Na_2SO_4, filtered, and concentrated under reduced pressure. The residue was purified by flash chromatography on silica gel (petroleum ether-EtOAc, 1:1) to give the target compound **14a**.

Target compounds **14b-v** were prepared with the same method and the corresponding substitute azide benzene (**13b-v**).

*4.1.6. (1S,5S)-2-((1-(2-hydroxyphenyl)-1H-1,2,3-triazol-4-yl)methyl)-1,8,8-trimethyl-2-azabicyclo[3.2.1]octan-3-one (**14a**).* A grey oil, yield: 72%. $[\alpha]_D^{25}$ = + 23.4 (c = 1.0 in EtOH). ^{1}H NMR (600 MHz, $CDCl_3$) δ 10.12 (s, 1H), 8.25 (s, 1H), 7.49 (dd, *J* = 8.1, 1.4 Hz, 1H), 7.28 (dd, *J* = 6.9, 1.3 Hz, 1H), 7.17 (dd, *J* = 8.2, 1.2 Hz, 1H), 7.00 – 6.96 (m, 1H), 4.81 (d, *J* = 15.3 Hz, 1H), 4.74 (d, *J* = 15.3 Hz, 1H), 2.73 (ddd, *J* = 18.2, 4.8, 2.5 Hz, 1H), 2.27 (dd, *J* = 18.1, 1.3 Hz, 1H), 2.04 (dd, *J* = 6.3, 3.8 Hz, 1H), 1.92 – 1.86 (m, 2H), 1.85 (dd, *J* = 11.6, 5.7 Hz, 1H), 1.45 (s, 3H), 1.43 (dd, *J* = 9.2, 5.7 Hz, 1H), 0.98 (s, 3H), 0.92 (s, 3H). ^{13}C NMR (150 MHz, $CDCl_3$) δ 171.92, 149.18, 145.50, 129.55, 122.99, 122.05, 120.20, 120.13, 119.03, 69.94, 44.69, 42.37, 39.94, 38.77, 37.45, 28.31, 25.05, 18.19, 17.50. ESI-HRMS calcd for $C_{19}H_{25}N_4O_2$ $[M + H]^+$ 341.19775, found: 341.19712. HPLC purity of 98.831% (retention time = 2.422).

*4.1.7. (1S,5S)-2-((1-(3-hydroxyphenyl)-1H-1,2,3-triazol-4-yl)methyl)-1,8,8-trimethyl-2-azabicyclo[3.2.1]octan-3-one (**14b**).* A brown oil, yield: 76%. $[\alpha]_D^{25}$ = + 43.9 (c = 1.0 in EtOH). ^{1}H NMR

(600 MHz, $CDCl_3$) δ 10.25 (s, 1H), 8.17 (s, 1H), 7.88 (t, *J* = 2.1 Hz, 1H), 7.34 (t, *J* = 8.1 Hz, 1H), 7.20 (dd, *J* = 7.9, 1.4 Hz, 1H), 6.97 (dd, *J* = 8.2, 1.8 Hz, 1H), 4.85 (d, *J* = 15.3 Hz, 1H), 4.73 (d, *J* = 15.2 Hz, 1H), 2.76 (ddd, *J* = 18.2, 4.8, 2.4 Hz, 1H), 2.35 – 2.28 (m, 1H), 2.07 – 2.01 (m, 1H), 1.93 – 1.88 (m, 2H), 1.84 (ddd, *J* = 13.8, 12.0, 5.4 Hz, 1H), 1.47 (dd, *J* = 9.4, 4.0 Hz, 1H), 1.44 (s, 3H), 0.97 (s, 3H), 0.91 (s, 3H). ^{13}C NMR (150 MHz, $CDCl_3$) δ 172.35, 158.64, 145.93, 137.62, 130.62, 121.78, 116.44, 110.50, 107.68, 70.15, 44.67, 42.27, 39.90, 38.71, 37.54, 28.31, 25.02, 18.16, 17.40. ESI-HRMS calcd for $C_{19}H_{25}N_4O_2$ $[M + H]^+$ 341.19775, found: 341.19748. HPLC purity of 98.047% (retention time = 2.814).

*4.1.8. (1S,5S)-2-((1-(4-hydroxyphenyl)-1H-1,2,3-triazol-4-yl)methyl)-1,8,8-trimethyl-2-azabicyclo[3.2.1]octan-3-one (**14c**).* A grey oil, yield: 74%. $[\alpha]_D^{25}$ = + 67.2 (c = 1.0 in EtOH). ^{1}H NMR (600 MHz, $CDCl_3$) δ 9.89 (s, 1H), 7.93 (s, 1H), 7.46 (d, *J* = 8.8 Hz, 2H), 6.98 (d, *J* = 8.8 Hz, 2H), 4.76 (dd, *J* = 38.6, 15.2 Hz, 2H), 2.81 – 2.73 (m, 1H), 2.31 (d, *J* = 18.2 Hz, 1H), 2.05 (s, 1H), 1.95 (ddd, *J* = 16.4, 9.7, 4.8 Hz, 2H), 1.91 – 1.84 (m, 1H), 1.52 (s, 3H), 1.49 – 1.42 (m, 1H), 1.00 (s, 3H), 0.93 (s, 3H). ^{13}C NMR (150 MHz, $CDCl_3$) δ 172.65, 158.13, 145.36, 129.36, 121.93, 121.90 (2C), 116.41 (2C), 70.32, 44.72, 42.23, 39.83, 38.92, 37.75, 28.39, 25.07, 18.19, 17.49. ESI-HRMS calcd for $C_{19}H_{25}N_4O_2$ $[M + H]^+$ 341.19775, found: 341.19700. HPLC purity of 97.913% (retention time = 2.325).

*4.1.9. (1S,5S)-1,8,8-trimethyl-1-((2-(o-tolyl)-1H-1,2,3-triazol-4-yl)methyl)-2-azabicyclo[3.2.1]octan-3-one (**14d**).* A grey oil, yield: 79%. $[\alpha]_D^{25}$ = + 28.4 (c = 1.0 in EtOH). ^{1}H NMR (600 MHz, $CDCl_3$) δ 7.79 (s, 1H), 7.41 – 7.37 (m, 1H), 7.35 (d, *J* = 7.4 Hz, 1H), 7.32 (dd, *J* = 3.9, 1.2 Hz, 2H), 4.85 (d, *J* = 15.3 Hz, 1H), 4.74 (d, *J* = 15.3 Hz, 1H), 2.72 (ddd, *J* = 18.1, 4.9, 2.5 Hz, 1H), 2.25 (dd, *J* = 18.1, 1.4 Hz, 1H), 2.18 (s, 3H), 2.04 (ddd, *J* = 9.3, 4.5, 2.4 Hz, 1H), 1.91 (t, *J* = 5.3 Hz, 1H), 1.89 – 1.80 (m, 2H), 1.45 (s, 3H), 1.44 – 1.41 (m, 1H), 0.98 (s, 3H), 0.92 (s, 3H). ^{13}C NMR (150 MHz, $CDCl_3$) δ 171.40, 145.78, 136.56, 133.52, 131.38, 129.71, 126.77, 125.95, 124.95, 69.71, 44.64, 42.49, 40.06, 38.70, 37.55, 28.34, 25.05, 18.14, 17.84, 17.53. ESI-HRMS calcd for $C_{20}H_{27}N_4O$ $[M + H]^+$ 339.21849, found: 339.21812. HPLC purity of 96.178% (retention time = 2.322).

*4.1.10. (1S,5S)-1,8,8-trimethyl-1-((2-(m-tolyl)-1H-1,2,3-triazol-4-yl)methyl)-2-azabicyclo[3.2.1]octan-3-one (**14e**).* A grey oil, yield: 81%. $[\alpha]_D^{25}$ = + 30.9 (c = 1.0 in EtOH). ^{1}H NMR (600 MHz, $CDCl_3$) δ 8.06 (s, 1H), 7.57 (s, 1H), 7.54 (d, *J* = 8.0 Hz, 1H), 7.37 (t, *J* = 7.8 Hz, 1H), 7.22 (d, *J* = 7.5 Hz, 1H), 4.76 (dd, *J* = 40.8, 15.2 Hz, 2H), 2.73 (dd, *J* = 18.1, 1.9 Hz, 1H), 2.43 (s, 3H), 2.26 (d, *J* = 18.0 Hz, 1H), 2.04 (s, 1H), 1.92 – 1.80 (m, 3H), 1.49 – 1.41 (m, 4H), 0.97 (s, 3H), 0.92 (s, 3H). ^{13}C NMR (150 MHz, $CDCl_3$) δ 171.52, 146.39, 139.84, 136.99, 129.44, 129.27, 121.51, 120.89, 117.35, 69.72, 44.64, 42.46, 40.03, 38.70, 37.52, 28.31, 25.05, 21.37, 18.18, 17.51. ESI-HRMS calcd for $C_{20}H_{27}N_4O$ $[M + H]^+$ 339.21849, found: 339.21807. HPLC purity of 98.729% (retention time = 2.325).

*4.1.11. (1S,5S)-1,8,8-trimethyl-1-((2-(p-tolyl)-1H-1,2,3-triazol-4-yl)methyl)-2-azabicyclo[3.2.1] octan-3-one (**14f**).* A brown oil, yield: 89%. $[\alpha]_D^{25}$ = + 32.4 (c = 1.0 in EtOH). ^{1}H NMR (600 MHz, $CDCl_3$) δ 8.04 (s, 1H), 7.62 (d, *J* = 8.1 Hz, 2H), 7.29 (d, *J* = 7.9 Hz, 2H), 4.75 (dd, *J* = 42.2, 15.2 Hz, 2H), 2.73 (d, *J* = 18.0 Hz, 1H), 2.41 (s, 3H), 2.26 (d, *J* = 18.1 Hz, 1H), 2.02 (d, *J* = 4.4 Hz, 1H), 1.94 – 1.86 (m, 2H), 1.83 (dd, *J* = 12.1, 5.1 Hz, 1H), 1.48 – 1.39 (m, 4H), 0.97 (s, 3H), 0.92 (s, 3H). ^{13}C NMR (150 MHz, $CDCl_3$) δ 171.54, 146.34, 138.61, 134.79, 130.14 (2C), 121.45, 120.19 (2C), 69.73, 44.65, 42.46, 40.03, 38.71, 37.54, 28.32, 25.06, 21.07, 18.18, 17.52. ESI-HRMS calcd for $C_{20}H_{27}N_4O$ $[M + H]^+$ 339.21849, found: 339.21826. HPLC purity of 98.181% (retention time = 2.327).

*4.1.12. (1S,5S)-2-((1-(2-methoxyphenyl)-1H-1,2,3-triazol-4-yl)methyl)-1,8,8-trimethyl-2-azabic yclo[3.2.1]octan-3-one (**14g**).* A grey oil, yield: 84%. $[\alpha]_D^{25}$ = + 23.8 (c = 1.0 in EtOH). ^{1}H NMR (600 MHz, $CDCl_3$) δ 8.10 (s, 1H), 7.74 (dd, *J* = 7.9, 1.6 Hz, 1H), 7.43 – 7.39 (m, 1H), 7.10 – 7.04 (m, 2H), 4.85 (d, *J* = 15.3 Hz, 1H), 4.75 (d, *J* = 15.3 Hz, 1H), 3.85 (s, 3H), 2.73 (ddd, *J* = 18.1, 4.9, 2.5 Hz, 1H), 2.26 (dd, *J* = 18.1, 1.3 Hz, 1H), 2.04 (s, 1H), 1.92 – 1.88 (m, 2H), 1.81 (ddd, *J* = 13.8, 12.0, 5.4 Hz, 1H), 1.47 – 1.43 (m, 1H), 1.42 (s, 3H), 0.97 (s, 3H), 0.95 (s, 3H). ^{13}C NMR (150 MHz, $CDCl_3$) δ 171.34, 151.16, 145.32, 130.00, 126.38, 125.44 (2C), 121.05, 112.12, 69.65, 55.90, 44.66, 42.49, 40.08, 38.63, 37.60, 28.36, 25.07, 18.13, 17.49. ESI-HRMS calcd for $C_{20}H_{27}N_4O_2$ $[M + H]^+$ 355.21340, found: 355.21283. HPLC purity of 95.873% (retention time = 2.345).

*4.1.13. (1S,5S)-2-((1-(3-methoxyphenyl)-1H-1,2,3-triazol-4-yl)methyl)-1,8,8-trimethyl-2-azabicyclo[3.2.1]octan-3-one (**14h**).* A grey oil, yield: 86%. $[\alpha]_D^{25}$ = + 47.1 (c = 1.0 in EtOH). ^{1}H NMR (600 MHz, $CDCl_3$) δ 8.07 (s, 1H), 7.39 (t, *J* = 8.1 Hz, 1H), 7.35 (s, 1H), 7.29 (t, *J* = 8.8 Hz, 1H), 6.97 – 6.92 (m, 1H), 4.76 (dd, *J* = 43.5, 15.2 Hz, 2H), 3.87 (s, 3H), 2.73 (dd, *J* = 18.0, 1.9 Hz, 1H), 2.26 (d, *J* = 18.1 Hz, 1H), 2.06 – 2.00 (m, 1H), 1.92 – 1.80 (m, 3H), 1.47 – 1.41 (m, 4H), 0.98 (s, 3H), 0.93 (s, 3H). ^{13}C NMR (150 MHz, $CDCl_3$) δ 171.48, 160.51, 146.46, 138.07, 130.42, 121.53, 114.58, 112.20, 105.87, 69.71, 55.62, 44.64, 42.45, 40.03, 38.70, 37.49, 28.31, 25.05, 18.18, 17.51. ESI-HRMS calcd for $C_{20}H_{27}N_4O_2$ $[M + H]^+$ 355.21340, found: 355.21268. HPLC purity of 94.876% (retention time = 2.362).

*4.1.14. (1S,5S)-2-((1-(4-methoxyphenyl)-1H-1,2,3-triazol-4-yl)methyl)-1,8,8-trimethyl-2-azabicyclo[3.2.1]octan-3-one (**14i**).* A grey oil, yield: 81%. $[\alpha]_D^{25}$ = + 27.6 (c = 1.0 in EtOH). ^{1}H NMR (600 MHz, $CDCl_3$) δ 7.99 (s, 1H), 7.64 (d, *J* = 9.0 Hz, 2H), 7.00 (d, *J* = 9.0 Hz, 2H), 4.78 (d, *J* = 15.2 Hz, 1H), 4.71 (d, *J* = 15.2 Hz, 1H), 3.86 (s, 3H), 2.73 (ddd, *J* = 18.1, 4.9, 2.5 Hz, 1H), 2.26 (dd, *J* = 18.1, 1.5 Hz, 1H), 2.05 (s, 1H), 1.92 – 1.86 (m, 2H), 1.82 (ddd, *J* = 13.8, 11.8, 5.4 Hz, 1H), 1.45 (s, 3H), 1.43 (dd, *J* = 9.4, 5.3 Hz, 1H), 0.98 (s, 3H), 0.93 (s, 3H). ^{13}C NMR (150 MHz, $CDCl_3$) δ 171.49, 159.64, 146.33, 130.59, 121.90 (2C), 121.59, 114.67 (2C), 69.72, 55.61, 44.66, 42.48, 40.05, 38.71, 37.55, 28.32, 25.06, 18.19, 17.53. ESI-HRMS calcd for $C_{20}H_{27}N_4O_2$ $[M + H]^+$ 355.21340, found: 355.21291. HPLC purity of 98.480% (retention time = 2.422).

*4.1.15. 2-(4-(((1S,5S)-1,8,8-trimethyl-3-oxo-2-azabicyclo[3.2.1]octan-2-yl)methyl)-1H-1,2,3-triazol-1-yl)benzonitrile (**14j**).* A brown oil, yield: 64%. $[\alpha]_D^{25}$ = + 32.9 (c = 1.0 in EtOH). ^{1}H NMR (600 MHz, $CDCl_3$) δ 8.20 (s, 1H), 7.86 (d, *J* = 7.9 Hz, 1H), 7.80 (d, *J* = 2.9 Hz, 2H), 7.61 (ddd, *J* = 8.5, 5.5, 3.2 Hz, 1H), 4.87 (d, *J* = 15.4 Hz, 1H), 4.74 (d, *J* = 15.4 Hz, 1H), 2.74 (ddd, *J* = 18.1, 4.6, 2.3 Hz, 1H), 2.27 (d, *J* = 18.1 Hz, 1H), 2.05 (s, 1H), 1.94 – 1.89 (m, 2H), 1.88 – 1.82 (m, 1H), 1.53 – 1.46 (m, 1H), 1.44 (s, 3H), 0.98 (d, *J* = 10.6 Hz, 6H). ^{13}C NMR (150 MHz, $CDCl_3$) δ 171.83, 146.77, 138.58, 134.26, 134.23, 129.59, 125.50, 124.00, 115.50, 107.19, 69.86, 44.69, 42.36, 39.95, 38.62, 37.56, 28.27, 25.04, 18.20, 17.46. ESI-HRMS calcd for $C_{20}H_{24}N_5O$ $[M + H]^+$ 350.19809, found: 350.19768. HPLC purity of 96.157% (retention time = 2.422).

*4.1.16. 3-(4-(((1S,5S)-1,8,8-trimethyl-3-oxo-2-azabicyclo[3.2.1]octan-2-yl)methyl)-1H-1,2,3-tri azol-1-yl)benzonitrile (**14k**).* A brown oil, yield: 70%. $[\alpha]_D^{25}$ = + 23.7 (c = 1.0 in EtOH). ^{1}H NMR (600 MHz, $CDCl_3$) δ 8.22 (s, 1H), 8.15 (s, 1H), 8.05 (d, *J* = 8.1 Hz, 1H), 7.71 (d, *J* = 7.7 Hz, 1H), 7.67 (t, *J* = 7.9 Hz, 1H), 4.80 (d, *J* = 15.2 Hz, 1H), 4.71 (d, *J* = 15.3 Hz, 1H), 2.73 (ddd, *J* = 18.1, 4.6, 2.3 Hz, 1H), 2.27 (d, *J* = 18.0 Hz, 1H), 2.05 (s, 1H), 1.92 (t, *J* = 5.2 Hz, 1H), 1.90 – 1.80 (m, 2H), 1.46 (s, 3H), 1.44 (dd, *J* = 9.3, 5.5 Hz, 1H), 0.99 (s, 3H), 0.93 (s, 3H). ^{13}C NMR (150 MHz, $CDCl_3$) δ 171.86, 146.99, 137.58, 131.82, 130.81, 124.18, 123.49, 121.64, 117.49, 114.02, 69.91, 44.67, 42.39, 39.94, 38.77, 37.49, 28.30, 25.06, 18.19, 14.20. ESI-HRMS calcd for $C_{20}H_{24}N_5O$ [M + H] $^+$ 350.19809, found: 350.19763. HPLC purity of 97.223% (retention time = 2.542).

*4.1.17. 4-(4-(((1S,5S)-1,8,8-trimethyl-3-oxo-2-azabicyclo[3.2.1]octan-2-yl)methyl)-1H-1,2,3-tri azol-1-yl)benzonitrile (**14l**).* A brown oil, yield: 67%. $[\alpha]_D^{25}$ = +27.8 (c = 1.0 in EtOH). ^{1}H NMR (600 MHz, $CDCl_3$) δ 8.19 (s, 1H), 7.95 (d, *J* = 8.6 Hz, 2H), 7.84 (d, *J* = 8.6 Hz, 2H), 4.80 (d, *J* = 15.3 Hz, 1H), 4.71 (d, *J* = 15.3 Hz, 1H), 2.72 (ddd, *J* = 18.0, 4.6, 2.3 Hz, 1H), 2.26 (d, *J* = 17.9 Hz, 1H), 2.05 (s, 1H), 1.94 – 1.91 (m, 1H), 1.90 – 1.80 (m, 2H), 1.46 (s, 3H), 1.43 (dd, *J* = 9.2, 5.5 Hz, 1H), 0.99 (s, 3H), 0.93 (s, 3H). ^{13}C NMR (150 MHz, $CDCl_3$) δ 171.56, 147.19, 139.84, 133.86 (2C), 121.45, 120.37 (2C), 117.79, 112.09, 69.78, 44.65, 42.41, 40.01, 38.72, 37.40, 28.29, 25.06, 18.18, 17.55. ESI-HRMS calcd for $C_{20}H_{24}N_5O$ [M + H] $^+$ 350.19809, found: 350.19793. HPLC purity of 98.325% (retention time = 2.362).

*4.1.18. (1S,5S)-2-((1-(2-fluorophenyl)-1H-1,2,3-triazol-4-yl)methyl)-1,8,8-trimethyl-2-azabicycl o[3.2.1]octan-3-one (**14m**).* A yellow oil, yield: 75%. $[\alpha]_D^{25}$ = + 25.8 (c = 1.0 in EtOH). ^{1}H NMR (600 MHz, $CDCl_3$) δ 8.11 (d, *J* = 2.7 Hz, 1H), 7.91 (td, *J* = 7.9, 1.1 Hz, 1H), 7.45 – 7.39 (m, 1H), 7.34 – 7.26 (m, 2H), 4.86 (d, *J* = 15.4 Hz, 1H), 4.73 (d, *J* = 15.3 Hz, 1H), 2.74 (ddd, *J* = 18.1, 4.6, 2.3 Hz, 1H), 2.27 (d, *J* = 18.0 Hz, 1H), 2.04 (s, 1H), 1.94 – 1.88 (m, 2H), 1.87 – 1.81 (m, 1H), 1.46 (dd, *J* = 9.5, 4.9 Hz, 1H), 1.43 (s, 3H), 0.98 (s, 3H), 0.94 (s, 3H). ^{13}C NMR (150 MHz, $CDCl_3$) δ 171.54, 153.38 (d, *J* = 251.4 Hz), 146.19, 130.13 (d, *J* = 7.8 Hz), 125.29 (d, *J* = 10.3 Hz), 125.08 (d, *J* = 3.8 Hz), 124.84, 124.56 (d, *J* = 7.8 Hz), 116.96 (d, *J* = 20.0 Hz), 69.70, 44.62, 42.39, 39.95, 38.63, 37.46, 28.27, 25.02, 18.10, 17.46. ESI-HRMS calcd for $C_{19}H_{24}FN_4O$ [M + H] $^+$

343.19341, found: 343.19314. HPLC purity of 97.942% (retention time = 2.364).

*4.1.19. (1S,5S)-2-((1-(3-fluorophenyl)-1H-1,2,3-triazol-4-yl)methyl)-1,8,8-trimethyl-2-azabicyclo[3.2.1]octan-3-one (**14n**).* A grey oil, yield: 78%. $[\alpha]_D^{25}$ = + 30.4 (c = 1.0 in EtOH). ^{1}H NMR (600 MHz, $CDCl_3$) δ 8.15 (s, 1H), 7.61 – 7.54 (m, 2H), 7.48 (dt, *J* = 14.1, 7.2 Hz, 1H), 7.12 (td, *J* = 8.2, 1.8 Hz, 1H), 4.80 (d, *J* = 15.3 Hz, 1H), 4.72 (d, *J* = 15.2 Hz, 1H), 2.73 (ddd, *J* = 18.0, 4.5, 2.2 Hz, 1H), 2.26 (d, *J* = 18.1 Hz, 1H), 2.04 (s, 1H), 1.93 – 1.87 (m, 2H), 1.86 – 1.81 (m, 1H), 1.46 (s, 3H), 1.43 (dd, *J* = 9.5, 5.3 Hz, 1H), 0.98 (s, 3H), 0.93 (s, 3H). ^{13}C NMR (150 MHz, $CDCl_3$) δ 171.63, 162.95 (d, *J* = 248.2 Hz), 146.56, 138.13 (d, *J* = 10.2 Hz), 131.07 (d, *J* = 9.0 Hz), 121.53, 115.50 (d, *J* = 3.2 Hz), 115.32 (d, *J* = 21.1 Hz), 107.92 (d, *J* = 26.3 Hz), 69.75, 44.58, 42.34, 39.90, 38.65, 37.39, 28.23, 24.97, 18.10, 17.43. ESI-HRMS calcd for $C_{19}H_{24}FN_4O$ $[M + H]^+$ 343.19341, found: 343.19286. HPLC purity of 96.725% (retention time = 2.538).

*4.1.20. (1S,5S)-2-((1-(4-fluorophenyl)-1H-1,2,3-triazol-4-yl)methyl)-1,8,8-trimethyl-2-azabicyclo[3.2.1]octan-3-one (**14o**).* A grey oil, yield: 75%. $[\alpha]_D^{25}$ = + 35.1 (c = 1.0 in EtOH). ^{1}H NMR (600 MHz, $CDCl_3$) δ 8.07 (s, 1H), 7.77 – 7.71 (m, 2H), 7.24 – 7.17 (m, 2H), 4.79 (d, *J* = 15.3 Hz, 1H), 4.71 (d, *J* = 15.3 Hz, 1H), 2.73 (ddd, *J* = 18.1, 4.8, 2.5 Hz, 1H), 2.26 (dd, *J* = 18.1, 1.3 Hz, 1H), 2.04 (s, 1H), 1.91 (d, *J* = 5.0 Hz, 1H), 1.90 – 1.82 (m, 2H), 1.46 (s, 3H), 1.43 (dd, *J* = 9.3, 5.2 Hz, 1H), 0.98 (s, 3H), 0.93 (s, 3H). ^{13}C NMR (150 MHz, $CDCl_3$) δ 171.54, 162.21 (d, *J* = 248.7 Hz), 146.52, 133.32 (d, *J* = 3.0 Hz), 122.19 (d, *J* = 8.5 Hz, 2C), 121.69, 116.54 (d, *J* = 23.2 Hz, 2C), 69.72, 44.60, 42.39, 39.96, 38.67, 37.43, 28.26, 25.00, 18.13, 17.47. ESI-HRMS calcd for $C_{19}H_{24}FN_4O$ $[M + H]^+$ 343.19341, found: 343.19282. HPLC purity of 98.306% (retention time = 2.416).

*4.1.21. (1S,5S)-2-((1-(2-chlorophenyl)-1H-1,2,3-triazol-4-yl)methyl)-1,8,8-trimethyl-2-azabicyclo[3.2.1]octan-3-one (**14p**).* A yellow oil, yield: 72%. $[\alpha]_D^{25}$ = + 17.7 (c = 1.0 in EtOH). ^{1}H NMR (600 MHz, $CDCl_3$) δ 8.00 (s, 1H), 7.61 – 7.58 (m, 1H), 7.57 – 7.54 (m, 1H), 7.46 – 7.41 (m, 2H), 4.87 (d, *J* = 15.3 Hz, 1H), 4.74 (d, *J* = 15.3 Hz, 1H), 2.73 (ddd, *J* = 18.1, 4.8, 2.4 Hz, 1H), 2.26 (d, *J* = 18.0 Hz, 1H), 2.08 – 2.02 (m, 1H), 1.93 – 1.88 (m, 2H), 1.84 (dd, *J* = 11.9, 5.4 Hz, 1H), 1.45 (dd, *J* = 9.4, 5.1 Hz, 1H), 1.43 (s, 3H), 0.98 (s, 3H), 0.94 (s, 3H). ^{13}C NMR (150 MHz, $CDCl_3$) δ

171.39, 145.82, 134.96, 130.69, 130.64, 128.72, 127.82, 127.76, 125.39, 69.68, 44.62, 42.43, 40.04, 38.59, 37.53, 28.30, 25.03, 18.14, 17.48. ESI-HRMS calcd for $C_{19}H_{24}ClN_4O$ $[M + H]^+$ 359.16386, found: 359.16345. HPLC purity of 98.440% (retention time = 2.378).

*4.1.22. (1S,5S)-2-((1-(3-chlorophenyl)-1H-1,2,3-triazol-4-yl)methyl)-1,8,8-trimethyl-2-azabicyclo[3.2.1]octan-3-one (**14q**).* A yellow oil, yield: 79%. $[\alpha]_D^{25}$ = + 32.5 (c = 1.0 in EtOH). ^{1}H NMR (600 MHz, $CDCl_3$) δ 8.11 (s, 1H), 7.82 (s, 1H), 7.66 (d, *J* = 8.0 Hz, 1H), 7.44 (t, *J* = 8.0 Hz, 1H), 7.39 (d, *J* = 8.0 Hz, 1H), 4.79 (d, *J* = 15.2 Hz, 1H), 4.71 (d, *J* = 15.1 Hz, 1H), 2.76 – 2.70 (m, 1H), 2.26 (d, *J* = 18.1 Hz, 1H), 2.05 (s, 1H), 1.93 – 1.82 (m, 3H), 1.45 (s, 3H), 1.43 (dd, *J* = 9.4, 5.5 Hz, 1H), 0.98 (s, 3H), 0.92 (s, 3H). ^{13}C NMR (150 MHz, $CDCl_3$) δ 171.66, 146.68, 137.88, 135.47, 130.75, 128.57, 121.57, 120.53, 118.21, 69.80, 44.65, 42.43, 40.00, 38.73, 37.46, 28.30, 25.05, 18.18, 17.52. ESI-HRMS calcd for $C_{19}H_{24}ClN_4O$ $[M + H]^+$ 359.16386, found: 359.16311. HPLC purity of 96.760% (retention time = 2.329).

*4.1.23. (1S,5S)-2-((1-(4-chlorophenyl)-1H-1,2,3-triazol-4-yl)methyl)-1,8,8-trimethyl-2-azabicyclo[3.2.1]octan-3-one (**14r**).* A yellow oil, yield: 77%. $[\alpha]_D^{25}$ = + 24.6 (c = 1.0 in EtOH). ^{1}H NMR (600 MHz, $CDCl_3$) δ 8.06 (s, 1H), 7.70 (d, *J* = 8.8 Hz, 2H), 7.48 (d, *J* = 8.8 Hz, 2H), 4.78 (d, *J* = 15.3 Hz, 1H), 4.70 (d, *J* = 15.1 Hz, 1H), 2.72 (ddd, *J* = 18.1, 4.8, 2.5 Hz, 1H), 2.25 (dd, *J* = 18.1, 1.2 Hz, 1H), 2.03 (dd, *J* = 6.9, 4.6 Hz, 1H), 1.92 – 1.82 (m, 3H), 1.45 (s, 3H), 1.43 (dd, *J* = 9.2, 5.3 Hz, 1H), 0.98 (s, 3H), 0.92 (s, 3H). ^{13}C NMR (150 MHz, $CDCl_3$) δ 171.52, 146.76, 135.58, 134.25, 129.83 (2C), 121.49, 121.45 (2C), 69.75, 44.67, 42.47, 40.05, 38.73, 37.48, 28.32, 25.08, 18.20, 17.56. ESI-HRMS calcd for $C_{19}H_{24}ClN_4O$ $[M + H]^+$ 359.16386, found: 359.16348. HPLC purity of 98.876% (retention time = 2.336).

*4.1.24. (1S,5S)-2-((1-(2-bromophenyl)-1H-1,2,3-triazol-4-yl)methyl)-1,8,8-trimethyl-2-azabicyclo[3.2.1]octan-3-one (**14s**).* A yellow oil, yield: 83%. $[\alpha]_D^{25}$ = + 22.7 (c = 1.0 in EtOH). ^{1}H NMR (600 MHz, $CDCl_3$) δ 7.96 (s, 1H), 7.73 (dd, *J* = 8.1, 1.2 Hz, 1H), 7.53 (dd, *J* = 7.9, 1.6 Hz, 1H), 7.47 (td, *J* = 7.7, 1.3 Hz, 1H), 7.38 (td, *J* = 7.8, 1.7 Hz, 1H), 4.87 (d, *J* = 15.4 Hz, 1H), 4.74 (d, *J* = 15.3 Hz, 1H), 2.73 (ddd, *J* = 18.1, 4.9, 2.5 Hz, 1H), 2.26 (dd, *J* = 18.1, 1.4 Hz, 1H), 2.04 (tdd, *J* = 7.4, 6.4, 3.7 Hz, 1H), 1.94 – 1.89 (m, 2H), 1.85 – 1.80 (m, 1H), 1.45 (dd, *J* = 9.3, 5.4 Hz, 1H),

1.43 (s, 3H), 0.98 (s, 3H), 0.94 (s, 3H). ^{13}C NMR (150 MHz, $CDCl_3$) δ 171.37, 145.85, 136.66, 133.80, 131.11, 128.42, 128.23, 125.46, 118.77, 69.71, 44.67, 42.48, 40.09, 38.61, 37.57, 28.35, 25.07, 18.25, 17.53. ESI-HRMS calcd for $C_{19}H_{24}BrN_4O$ $[M + H]^+$ 403.11335, found: 403.11224. HPLC purity of 98.533% (retention time = 2.368).

*4.1.25. (1S,5S)-2-((1-(3-bromophenyl)-1H-1,2,3-triazol-4-yl)methyl)-1,8,8-trimethyl-2-azabicyclo[3.2.1]octan-3-one (**14t**).* A yellow oil, yield: 77%. $[\alpha]_D^{25}$ = + 23.0 (c = 1.0 in EtOH). ^{1}H NMR (600 MHz, $CDCl_3$) δ 8.18 (s, 1H), 7.98 (s, 1H), 7.73 (d, *J* = 8.0 Hz, 1H), 7.52 (d, *J* = 8.0 Hz, 1H), 7.38 (t, *J* = 8.1 Hz, 1H), 4.79 (d, *J* = 15.3 Hz, 1H), 4.72 (d, *J* = 15.2 Hz, 1H), 2.73 (dd, *J* = 18.1, 2.2 Hz, 1H), 2.26 (d, *J* = 18.2 Hz, 1H), 2.04 (s, 1H), 1.90 (s, 1H), 1.89 – 1.80 (m, 2H), 1.45 (s, 3H), 1.42 (dd, *J* = 9.4, 5.3 Hz, 1H), 0.98 (s, 3H), 0.92 (s, 3H). ^{13}C NMR (150 MHz, $CDCl_3$) δ 171.50, 146.52, 137.84, 131.33, 130.93, 123.11, 123.03, 121.47, 118.56, 69.66, 44.52, 42.29, 39.85, 38.61, 37.34, 28.19, 24.94, 18.07, 17.39. ESI-HRMS calcd for $C_{19}H_{24}BrN_4O$ $[M + H]^+$ 403.11335, found: 403.11306. HPLC purity of 98.269% (retention time = 2.377).

*4.1.26. (1S,5S)-2-((1-(4-bromophenyl)-1H-1,2,3-triazol-4-yl)methyl)-1,8,8-trimethyl-2-azabicyclo[3.2.1]octan-3-one (**14u**).* A yellow oil, yield: 80%. $[\alpha]_D^{25}$ = + 21.2 (c = 1.0 in EtOH). ^{1}H NMR (600 MHz, $CDCl_3$) δ 8.07 (s, 1H), 7.68 – 7.60 (m, 4H), 4.78 (d, *J* = 15.2 Hz, 1H), 4.70 (d, *J* = 15.2 Hz, 1H), 2.72 (dd, *J* = 18.1, 1.9 Hz, 1H), 2.25 (d, *J* = 18.1 Hz, 1H), 2.07 – 2.01 (m, 1H), 1.90 (d, *J* = 7.2 Hz, 1H), 1.88 – 1.79 (m, 2H), 1.45 (s, 3H), 1.43 (dd, *J* = 9.1, 5.4 Hz, 1H), 0.98 (s, 3H), 0.92 (s, 3H). ^{13}C NMR (150 MHz, $CDCl_3$) δ 171.57, 146.77, 136.05, 132.80 (2C), 122.13, 121.70 (2C), 121.44, 69.77, 44.67, 42.47, 40.04, 38.75, 37.49, 28.32, 25.08, 18.21, 17.56. ESI-HRMS calcd for $C_{19}H_{24}BrN_4O$ $[M + H]^+$ 403.11335, found: 403.11206. HPLC purity of 98.628% (retention time = 2.328).

*4.1.27. (1S,5S)-1,8,8-trimethyl-2-((1-phenyl-1H-1,2,3-triazol-4-yl)methyl)-2-azabicyclo[3.2.1]octan-3-one (**14v**).* A brown oil, yield: 87%. $[\alpha]_D^{25}$ = + 33.7 (c = 1.0 in EtOH). ^{1}H NMR (600 MHz, $CDCl_3$) δ 8.13 (s, 1H), 7.76 (d, *J* = 8.1 Hz, 2H), 7.49 (t, *J* = 7.9 Hz, 2H), 7.39 (t, *J* = 7.4 Hz, 1H), 4.80 (d, *J* = 15.3 Hz, 1H), 4.73 (d, *J* = 15.3 Hz, 1H), 2.75 – 2.69 (m, 1H), 2.25 (d, *J* = 18.1 Hz, 1H), 2.03 (s, 1H), 1.91 – 1.85 (m, 2H), 1.84 – 1.79 (m, 1H), 1.45 (s, 3H), 1.44 – 1.39 (m, 1H),

0.96 (s, 3H), 0.92 (s, 3H). ^{13}C NMR (150 MHz, $CDCl_3$) δ 171.36, 146.32, 136.91, 129.53 (2C), 128.40, 121.34, 120.08 (2C), 69.58, 44.50, 42.30, 39.88, 38.56, 37.36, 28.19, 24.92, 18.05, 17.38. ESI-HRMS calcd for $C_{19}H_{25}N_4O$ $[M + H]^+$ 325.20284, found: 325.20266. HPLC purity of 97.794% (retention time = 2.585).

4.2. Biology

4.2.1. Cell culture

All cancer cell lines were obtained from the American Type Culture Collection (ATCC). All healthy cell lines were obtained from the Shanghai Cell Resource Bank. Cultured cells using the culture guidelines provided by the supplier and performed relevant mycoplasma tests once a month.

4.2.2. MTT assay

The cultured cells were collected in the logarithmic growth phase, digested with 0.25% trypsin, and diluted into a single cell suspension with phosphate-buffered saline (PBS). Then 100 µL of each cell type (4×10^4 cells/mL) was seeded into 96-well plate and incubated for 24 h. Different concentrations of compounds were added into the 96-well plates. Respective concentrations of DMSO were used as control. Then these plates were incubated for 24 h, and 20 µL MTT solution (5 mg/mL) (Wuhan Bost Biotechnology Co., Ltd., China) was added and cultured for 4 h. The nutrient solution was discarded slowly and 100 µL of DMSO was added to each well. The optical density (OD) of each well was detected at 490 nm using a microplate reader. The IC_{50} value was determined as the inhibitor's concentration, which produced 50% inhibition calculated IC_{50} values for the compounds using probability units and weighted regression methods. Determined the CC_{50} value as the concentration of the compound at which 50% of the healthy cell died. Every assay was performed in triplicate. Data are presented as the mean ± SD (n = 3).

4.2.3. Inhibition of heat shock protein 90

Fluorescence polarization assay was used to screen target compounds for their inhibition effects for Hsp90α. Briefly, various concentrations of compounds and fluorescein isothiocyanate-labeled geldanamycin were added to each 96-well plate. Recombinant Hsp90α

protein (ProSpec-Tany Company, China) was diluted with the reaction buffer (20 mM HEPES pH 7.3, 50 mM KCl, 5 mM $MgCl_2$, 20 mM Na_2MoO_4, 0.01% Triton X-100, 100 μg/mL bovine serum albumin, and 2 mM dithiothreitol) and added to each well to get the final concentration of 22.2 nM. The enzyme reaction was initiated as soon as the Hsp90α protein was added. After incubation for 60 min at 4 °C, the fluorescent polarization values were measured at an excitation wavelength at 495 nm and an emission wavelength at 530 nm.

4.2.4. Molecular docking study

Molecular modeling studies were carried out with MOE (Molecular Operating Environment, Version 2015.10) software [48]. The crystal structure of Hsp90α (PDB ID: 2XJX, Resolution 1.66 Å) downloaded from RCSB Protein Data Bank was adopted in docking calculations [2]. The receptor was optimized by a Quickprep protocol with the following procedures of Structure Preparation, Protonate 3D and Structure Refine (RMSD gradient = 0.1 kcal/mol, AMBER10: EHT field) [49, 50]. The docking procedure was adopted the standard protocol implemented in MOE and all parameters were maintained as the defaults. The binding interactions are illustrated by PyMOL software [51].

4.2.5. Cell cycle analysis

LoVo and SW620 cells (2×10^5 cells) were incubated in 6 cm dishes for 24 h. Then **14t** was added to the dishes with different concentrations. After incubation for 24 h, the cells were harvested and fixed in 80% ethanol at 4 °C overnight, and then incubated with the DNA-interacting dye propidium iodide (PI) (Promega Corporation, USA) for 30 min at 37 °C. Cell cycle analysis was performed using a flow cytometry (Becton Dickinson and Company, USA).

4.2.6. Annexin V/propidium iodide (PI) staining

The Annexin V-FITC/PI dual staining assay was used to determine the percentage of apoptotic cells. Briefly, 1 mL of LoVo and SW620 cells (1×10^6 cells/mL) were plated in 6-well plates and incubated for 24 h. Then **14t** was added to the cells with indicated concentrations. After another incubation of 24 h, the cells were harvested softly and washed twice with cold PBS. Then

the cells were re-suspended in 150 μL of PBS, 10 μLof fluorescein isothiocyanate (FITC)-labeled Annexin V (Annexin V-FITC) (Promega Corporation, USA) and 5 μL of PI were added. The mixture was incubated at room temperature for 10 min in the dark and then analyzed by flow cytometry (Becton Dickinson and Company, USA).

4.2.7. Western blot analysis

LoVo and SW620 cells (1×10^7 cells) were seeded into the flask (Becton Dickinson and Company, USA), and these cells were incubated with different concentrations of **14t** for 24 h. Then the cells were lysed, and the proteins were extracted. Extracted proteins were separated from each other using polyacrylamide electrophoresis on a 10% gel (Beyotime Biotechnology Company, China) and transferred to a polyvinylidene fluoride (PVDF) membrane (Bio-Rad Company, USA), followed by incubated with the primary specific antibodies (bax, bcl-2, cleaved-caspase 3, caspase 3 and β-actin). After binding of appropriate secondary antibodies, proteins were visualized with an ECL detection system.

4.2.8. Cell migration and wound healing assays

Cell migratory ability was measured using transwell chambers (8-μm pore size; Corning Costar, USA). For the transwell assay, LoVo and SW620 cells suspended in serum-free RPMI-1640 medium containing different concentrations of **14t** were seeded into the upper chamber. The lower chamber contained RPMI-1640 medium supplemented with 20% serum. After 24 h incubation, the filters were fixed in methanol and stained with 0.1% crystal violet. The upper faces of the filters were gently abraded, and the lower faces with cells migrated across the filters were imaged and counted under the microscope. For wound healing assay, cells were placed into 6-well plates and cultured until 100% confluence. An artificial scratch was created using a 200 μL pipette tip. Add serum-free RPMI-1640 medium containing different concentrations of **14t**. At 24 h after culturing in serum-free medium, wound closure images were captured in the same field under magnification. Cell healing rates were calculated by the fraction of cell coverage across the line. These experiments were performed in triplicate and repeated three times.

4.2.9. Evaluation of in vivo antitumor activity

All animal experimental protocols were approved by the Laboratory Animal Welfare and Ethical Committee of China Medical University. Five-week-old immunodeficient BABL/c female nude mice, weighing 18 to 20 g, were purchased and maintained under specific pathogen-free conditions. SW620 cells (1×10^7 cells) were injected subcutaneously into the right flank of nude mice. When the tumor reached a volume of about 50 mm^3, the mice were randomized to drug-treated or vehicle groups (five mice per group). Tumor growth was measured every 3 days using a vernier caliper. For a total of 21 days, the mice were injected intraperitoneally with compound **14t** and 17-AAG (5 mg/kg) every day, after which the mice were euthanized and the xenograft tumors were dissected. As controls, vehicle groups of five mice were treated with the PBS. The tumor volume (V) was calculated using the formula: V (mm^3) = (length × $width^2$)/2. The tumor growth inhibition (TGI) values were calculated by the following formula: TGI (%) = [1–RTV (drug–treated)/RTV (control)] × 100%, The individual relative tumor volume: RTV = (tumor volume on day 21)/(tumor volume on day 1).

4.2.10. Immunohistochemistry

Sections derived from formalin-fixed and paraffin-embedded mouse tissues were deparaffinized by incubation overnight at 65 °C followed by rehydration in sequential xylene and ethanol rinses. After incubation with hydrogen peroxide, the slides were washed with PBS and then incubated with 0.4% Triton X-100. The sections were incubated with blocking solution (Dako Protein Block, Denmark) for 30 min at room temperature after washing with PBS. The sections were further incubated with primary antibodies (Ki67 and cleaved-caspase 3) overnight at 4 °C, washed with PBS several times, incubated with the corresponding biotinylated secondary antibodies, and then washed with PBS multiple times. After adding avidin-biotin complexes, the sections were visualized using diaminobenzidine (DAB) detection reagent (Enzo Life Sciences, USA) and mounted with a mounting solution (Vector Laboratories, USA).

Acknowledgements

This work was supported by the National Natural Science Foundation of China (Grant Nos. 81803355 and 81573687), the Scientific Research Fund of Liaoning Provincial Education Department (LQNK201739), the Key Research and Development Project of Liaoning (2019 NO.

26) and the Doctoral Research Funding (229181).

Appendix A. Supplementary data

Supplementary data to this article can be found online.

References

[1] P. LaPointe, R. Mercier, A. Wolmarans, Aha-type co-chaperones: the alpha or the omega of the Hsp90 ATPase cycle, Biol. Chem. 401 (2020) 423-434. https://doi.org/10.1515/hsz-2019-0341.

[2] S.Y. Park, Y.J. Oh, Y. Lho, J.H. Jeong, K.H. Liu, J. Song, S.H. Kim, E. Ha, Y.H. Seo, Design, synthesis, and biological evaluation of a series of resorcinol-based *N*-benzyl benzamide derivatives as potent Hsp90 inhibitors, Eur. J. Med. Chem. 143 (2018) 390-401. https://doi.org/10.1016/j.ejmech.2017.11.054.

[3] D.T. Gewirth, Paralog Specific Hsp90 Inhibitors - A Brief History and a Bright Future, Curr. Top. Med. Chem. 16 (2016) 2779-2791. https://doi.org/10.2174/1568026616666160413141154.

[4] Y.C. Yang, T.Y. Cheng, S.M. Huang, C.Y. Su, P.W. Yang, J.M. Lee, C.K. Chen, M. Hsiao, K.T. Hua, M.L. Kuo, Cytosolic PKM2 stabilizes mutant EGFR protein expression through regulating HSP90-EGFR association, Oncogene 36 (2017) 4234. https://doi.org/10.1038/onc.2017.18.

[5] M. Pool, A.G.T. Terwisscha van Scheltinga, A. Kol, D. Giesen, E.G.E. de Vries, M.N. Lub-de Hooge, (89)Zr-Onartuzumab PET imaging of c-MET receptor dynamics, Eur. J. Nucl. Med. Mol. Imaging 44 (2017) 1328-1336. https://doi.org/10.1007/s00259-017-3672-x.

[6] J.Y. Ahn, J.S. Lee, H.Y. Min, H.Y. Lee, Acquired resistance to 5-fluorouracil via HSP90/Src-mediated increase in thymidylate synthase expression in colon cancer, Oncotarget 6 (2015) 32622-32633. https://doi.org/10.18632/oncotarget.5327.

[7] X. Sun, Y. Sun, P. Jiang, G. Qi, X. Chen, Crosstalk between endothelial cell-specific calpain inhibition and the endothelial-mesenchymal transition via the HSP90/Akt signaling pathway, Biomed. Pharmacother. 124 (2020) 109822. https://doi.org/10.1016/j.biopha.2020.109822.

[8] H.S. Kim, M. Hong, J. Ann, S. Yoon, C.T. Nguyen, S.C. Lee, H.Y. Lee, Y.G. Suh, J.H. Seo, H. Choi, J.Y. Kim, K.W. Kim, J. Kim, Y.M. Kim, S.J. Park, H.J. Park, J. Lee, Synthesis and biological evaluation of C-ring truncated deguelin derivatives as heat shock protein 90 (HSP90) inhibitors, Bioorg. Med. Chem. 24 (2016) 6082-6093. https://doi.org/10.1016/j.bmc.2016.09.067.

[9] D.J. Chang, H. An, K.S. Kim, H.H. Kim, J. Jung, J.M. Lee, N.J. Kim, Y.T. Han, H. Yun, S. Lee, G. Lee, S. Lee, J.S. Lee, J.H. Cha, J.H. Park, J.W. Park, S.C. Lee, S.G. Kim, J.H. Kim, H.Y. Lee, K.W. Kim, Y.G. Suh, Design, synthesis, and biological evaluation of novel deguelin-based heat shock protein 90 (HSP90) inhibitors targeting proliferation and angiogenesis, J. Med. Chem. 55 (2012) 10863-10884. https://doi.org/10.1021/jm301488q.

[10] R. Suzuki, T. Hideshima, N. Mimura, J. Minami, H. Ohguchi, S. Kikuchi, Y. Yoshida, G. Gorgun, D. Cirstea, F. Cottini, J. Jakubikova, Y.T. Tai, D. Chauhan, P.G. Richardson, N.C. Munshi, T. Utsugi, K.C. Anderson, Anti-tumor activities of selective HSP90α/β inhibitor, TAS-116, in combination with bortezomib in multiple myeloma, Leukemia 29 (2015) 510-514. https://doi.org/10.1038/leu.2014.300.

[11] C. Liang, H. Hao, X. Wu, Z. Li, J. Zhu, C. Lu, Y. Shen, Design and synthesis of *N*-(5-chloro-2,4-dihydroxybenzoyl)-(*R*)-1,2,3,4-tetrahydroisoquinoline-3-carboxamides as novel Hsp90 inhibitors, Eur. J. Med. Chem. 121 (2016) 272-282. https://doi.org/10.1016/j.ejmech.2016.05.033.

[12] R. Ojha, K. Nepali, C.H. Chen, K.H. Chuang, T.Y. Wu, T.E. Lin, K.C. Hsu, M.W. Chao, M.J. Lai, M.H. Lin, H.L. Huang, C.D. Chang, S.L. Pan, M.C. Chen, J.P. Liou, Isoindoline scaffold-based dual inhibitors of HDAC6 and HSP90 suppressing the growth of lung cancer *in vitro* and *in vivo*, Eur. J. Med. Chem. 190 (2020) 112086. https://doi.org/10.1016/j.ejmech.2020.112086.

[13] T. Uno, Y. Kawai, S. Yamashita, H. Oshiumi, C. Yoshimura, T. Mizutani, T. Suzuki, K.T. Chong, K. Shigeno, M. Ohkubo, Y. Kodama, H. Muraoka, K. Funabashi, K. Takahashi, S. Ohkubo, M. Kitade, Discovery of 3-Ethyl-4-(3-isopropyl-4-(4-(1-methyl-1*H*-pyrazol-4-yl)-1*H*-imidazol-1-yl)-1*H*-pyrazolo[3,4-b]pyridin-1-yl)benzamide (TAS-116) as a Potent, Selective, and Orally Available HSP90 Inhibitor, J. Med. Chem. 62 (2019) 531-551. https://doi.org/10.1021/acs.jmedchem.8b01085.

[14] J.D. Huck, N.L.S. Que, R.M. Immormino, L. Shrestha, NECA derivatives exploit the paralog-specific properties of the site 3 side pocket of Grp94, the endoplasmic reticulum Hsp90, J. Biol. Chem. 294 (2019) 16010-16019. https://doi.org/10.1074/jbc.RA119.009960.

[15] J.T. Ernst, M. Liu, H. Zuccola, T. Neubert, K. Beaumont, A. Turnbull, A. Kallel, B. Vought, D. Stamos, Correlation between chemotype-dependent binding conformations of HSP90α/β and isoform selectivity-Implications for the structure-based design of HSP90α/β selective inhibitors

for treating neurodegenerative diseases, Bioorg. Med. Chem. Lett. 24 (2014) 204-208. https://doi.org/10.1016/j.bmcl.2013.11.036.

[16] O.W. Mak, R. Chand, J. Reynisson, Identification of Isoform-Selective Ligands for the Middle Domain of Heat Shock Protein 90 (Hsp90), Int. J. Mol. Sci. 20 (2019) 5333. https://doi.org/10.3390/ijms20215333.

[17] L.H. Pearl, C. Prodromou, Structure and *in vivo* function of Hsp90, Curr. Opin. Struct. Biol. 10 (2000) 46-51. https://doi.org/10.1016/S0959-440X(99)00047-0.

[18] L. Whitesell, E.G. Mimnaugh, B. De Costa, C.E. Myers, L.M. Neckers, Inhibition of heat shock protein HSP90-pp60v-src heteroprotein complex formation by benzoquinone ansamycins: essential role for stress proteins in oncogenic transformation, Proc. Natl. Acad. Sci. U. S. A. 91 (1994) 8324-8328. https://doi.org/10.1073/pnas.91.18.8324.

[19] J.R. Infante, G.J. Weiss, S. Jones, R. Tibes, T.M. Bauer, J.C. Bendell, J.M. Hinson, Jr., D.D. Von Hoff, H.A. Burris, 3rd, E.O. Orlemans, R.K. Ramanathan, Phase I dose-escalation studies of SNX-5422, an orally bioavailable heat shock protein 90 inhibitor, in patients with refractory solid tumours, Eur. J. Cancer 50 (2014) 2897-2904. https://doi.org/10.1016/j.ejca.2014.07.017.

[20] S.M. Roe, C. Prodromou, R. O'Brien, J.E. Ladbury, P.W. Piper, L.H. Pearl, Structural basis for inhibition of the Hsp90 molecular chaperone by the antitumor antibiotics radicicol and geldanamycin, J. Med. Chem. 42 (1999) 260-266. https://doi.org/10.1021/jm980403y.

[21] T.W. Schulte, L.M. Neckers, The benzoquinone ansamycin 17-allylamino-17-demethoxygeldanamycin binds to HSP90 and shares important biologic activities with geldanamycin, Cancer Chemother. Pharmacol. 42 (1998) 273-279. https://doi.org/10.1007/s002800050817.

[22] J.D. Eskew, T. Sadikot, P. Morales, A. Duren, I. Dunwiddie, M. Swink, X. Zhang, S. Hembruff, A. Donnelly, R.A. Rajewski, B.S. Blagg, J.R. Manjarrez, R.L. Matts, J.M. Holzbeierlein, G.A. Vielhauer, Development and characterization of a novel C-terminal inhibitor of Hsp90 in androgen dependent and independent prostate cancer cells, BMC Cancer 11 (2011) 468. https://doi.org/10.1186/1471-2407-11-468.

[23] J.A. Burlison, L. Neckers, A.B. Smith, A. Maxwell, B.S. Blagg, Novobiocin: redesigning a DNA gyrase inhibitor for selective inhibition of hsp90, J. Am. Chem. Soc. 128 (2006) 15529-15536. https://doi.org/10.1021/ja065793p.

[24] L. Whitesell, S.L. Lindquist, HSP90 and the chaperoning of cancer, Nat. Rev. Cancer 5 (2005) 761-772. https://doi.org/10.1038/nrc1716.

[25] S. Dutta Gupta, M.K. Bommaka, A. Banerjee, Inhibiting protein-protein interactions of Hsp90 as a novel approach for targeting cancer, Eur. J. Med. Chem. 178 (2019) 48-63. https://doi.org/10.1016/j.ejmech.2019.05.073.

[26] S. Wang, G. Dong, C. Sheng, Structural Simplification of Natural Products, Chem. Rev. 119 (2019) 4180-4220. https://doi.org/10.1021/acs.chemrev.8b00504.

[27] J. Gudin, J. Fudin, S. Nalamachu, Levorphanol use: past, present and future, Postgrad. Med. 128 (2016) 46-53. https://doi.org/10.1080/00325481.2016.1128308.

[28] J. Liu, R. Ma, F. Bi, F. Zhang, C. Hu, H. Venter, S.J. Semple, S. Ma, Novel 5-methyl-2-phenylphenanthridium derivatives as FtsZ-targeting antibacterial agents from structural simplification of natural product sanguinarine, Bioorg. Med. Chem. Lett. 28 (2018) 1825-1831. https://doi.org/10.1016/j.bmcl.2018.04.015.

[29] V.A. Steadman, S.B. Pettit, K.G. Poullennec, L. Lazarides, A.J. Keats, D.K. Dean, S.J. Stanway, C.A. Austin, J.A. Sanvoisin, G.M. Watt, H.G. Fliri, A.C. Liclican, D. Jin, M.H. Wong, S.A. Leavitt, Y.J. Lee, Y. Tian, C.R. Frey, T.C. Appleby, U. Schmitz, P. Jansa, R.L. Mackman, Discovery of Potent Cyclophilin Inhibitors Based on the Structural Simplification of Sanglifehrin A, J. Med. Chem. 60 (2017) 1000-1017. https://doi.org/10.1021/acs.jmedchem.6b01329.

[30] P.R. Blakemore, J.D. White, Morphine, the Proteus of organic molecules, Chem. Commun. 11 (2002) 1159-1168. https://doi.org/10.1039/b111551k.

[31] M.Y. Ren, Q.T. Yu, C.Y. Shi, J.B. Luo, Anticancer Activities of C(18)-, C(19)-, C(20)-, and Bis-Diterpenoid Alkaloids Derived from Genus Aconitum, Molecules 22 (2017) 267. https://doi.org/10.3390/molecules22020267.

[32] L. Zhu, J. Wu, M. Zhao, W. Song, X. Qi, Y. Wang, L. Lu, Z. Liu, Mdr1a plays a crucial role in regulating the analgesic effect and toxicity of aconitine by altering its pharmacokinetic characteristics, Toxicol. Appl. Pharmacol. 320 (2017) 32-39. https://doi.org/10.1016/j.taap.2017.02.008.

[33] J.W. Liang, T.J. Zhang, Z.J. Li, Z.X. Chen, F.H. Meng, Predicting potential antitumor targets of Aconitum alkaloids by molecular docking and protein–ligand interaction fingerprint, Med. Chem. Res. 25 (2016) 1115-1124. https://doi.org/10.1007/s00044-016-1553-7.

[34] N.A. Doering, K.G.M. Kou, K. Norseeda, J.C. Lee, C.J. Marth, G.M. Gallego, R. Sarpong, A Copper-Mediated Conjugate Addition Approach to Analogues of Aconitine-Type Diterpenoid Alkaloids, J. Org. Chem. 83 (2018) 12911-12920. https://doi.org/10.1021/acs.joc.8b01967.

[35] C. Luo, F. Yi, Y. Xia, Z. Huang, X. Zhou, X. Jin, J. Yi, Y. Tang, Comprehensive quality evaluation of the lateral root of Aconitum carmichaelii Debx. (Fuzi): Simultaneous determination of nine alkaloids and chemical fingerprinting coupled with chemometric analysis, J. Sep. Sci. 42 (2018) 980-990. https://doi.org/10.1002/jssc.201800937.

[36] M.Y. Wang, J.W. Liang, K.M. Olounfeh, Q. Sun, N. Zhao, F.H. Meng, A Comprehensive In Silico Method to Study the QSTR of the Aconitine Alkaloids for Designing Novel Drugs, Molecules 23 (2018) 2385. https://doi.org/10.3390/molecules23092385.

[37] E. Nyirimigabo, Y. Xu, Y. Li, Y. Wang, K. Agyemang, Y. Zhang, A review on phytochemistry, pharmacology and toxicology studies of Aconitum, J. Pharm. Pharmacol. 67 (2015) 1-19. https://doi.org/10.1111/jphp.12310.

[38] K. Wada, E. Ohkoshi, Y. Zhao, M. Goto, S.L. Morris-Natschke, K.H. Lee, Evaluation of Aconitum diterpenoid alkaloids as antiproliferative agents, Bioorg. Med. Chem. Lett. 25 (2015) 1525-1531. https://doi.org/10.1016/j.bmcl.2015.02.018.

[39] F.H. Meng, Y. Zhang, T.J. Zhang, S. Tu, X.Y. Li, L. Wang, Q. Sun, J.W. Liang, N. Zhao, Azabicyclo[3.2.1]octan-3-one compound and its preparation method, application in preparation of anti-tumor drug, Faming Zhuanli Shenqing (2019) CN 110183455A. https://worldwide.espacenet.com/patent/search?q=pn%3DCN110183455A.

[40] E. Kotsikorou, F. Navas, 3rd, M.J. Roche, A.F. Gilliam, B.F. Thomas, H.H. Seltzman, P. Kumar, Z.H. Song, D.P. Hurst, D.L. Lynch, P.H. Reggio, The importance of hydrogen bonding and aromatic stacking to the affinity and efficacy of cannabinoid receptor CB2 antagonist, 5-(4-chloro-3-methylphenyl)-1-[(4-methylphenyl)methyl]-*N*-[(1*S*,2*S*,4*R*)-1,3,3-trimethylbicyclo[2.2.1]hept-2-yl]-1*H*-pyrazole-3-carboxamide (SR144528), J. Med. Chem. 56 (2013) 6593-6612. https://doi.org/10.1021/jm400070u.

[41] P. Deslongchamps, A. Bélanger, D.J.F. Berney, H.J. Borschberg, P. Soucy, The total synthesis of (+)-ryanodol. Part III. Preparation of (+)-anhydroryanodol from a key pentacyclic intermediate, Can. J. Chem. 68 (2011) 153-185. https://doi.org/10.1139/v90-023.

[42] L. Yuan, S. Zhang, J. Peng, Y. Li, Q. Yang, Synthetic surfactin analogues have improved

anti-PEDV properties, PLoS One 14 (2019) e0215227. https://doi.org/10.1371/journal.pone.0215227.

[43] Y. Yao, X.Y. Jia, H.Y. Tian, Y.X. Jiang, G.J. Xu, Q.J. Qian, F.K. Zhao, Comparative proteomic analysis of colon cancer cells in response to oxaliplatin treatment, Biochim. Biophys. Acta 1794 (2009) 1433-1440. https://doi.org/10.1016/j.bbapap.2009.06.005.

[44] Q. Li, H. Chen, Epigenetic modifications of metastasis suppressor genes in colon cancer metastasis, Epigenetics 6 (2011) 849-852. https://doi.org/10.4161/epi.6.7.16314.

[45] J. Chen, F.L. Wang, W.D. Chen, Modulation of apoptosis-related cell signalling pathways by curcumin as a strategy to inhibit tumor progression, Mol. Biol. Rep. 41 (2014) 4583-4594. https://doi.org/10.1007/s11033-014-3329-9.

[46] A.M. Sharifi, S.H. Mousavi, M. Jorjani, Effect of chronic lead exposure on pro-apoptotic Bax and anti-apoptotic Bcl-2 protein expression in rat hippocampus *in vivo*, Cell. Mol. Neurobiol. 30 (2010) 769-774. https://doi.org/10.1007/s10571-010-9504-1.

[47] L.G. Rodriguez, X. Wu, J.L. Guan, Wound-healing assay, Methods Mol. Biol. 294 (2005) 23-29. https://doi.org/10.1385/1-59259-860-9:023.

[48] S. Vilar, G. Cozza, S. Moro, Medicinal chemistry and the molecular operating environment (MOE): application of QSAR and molecular docking to drug discovery, Curr. Top. Med. Chem. 8 (2008) 1555-1572. https://doi.org/10.2174/156802608786786624.

[49] S.H. Abbas, D. Abuo-Rahma Gel, M. Abdel-Aziz, O.M. Aly, E.A. Beshr, A.M. Gamal-Eldeen, Synthesis, cytotoxic activity, and tubulin polymerization inhibitory activity of new pyrrol-2(3*H*)-ones and pyridazin-3(2*H*)-ones, Bioorg. Chem. 66 (2016) 46-62. https://doi.org/10.1016/j.bioorg.2016.03.007.

[50] T.J. Zhang, Y. Zhang, S. Tu, Y.H. Wu, Z.H. Zhang, F.H. Meng, Design, synthesis and biological evaluation of *N*-(3-(1*H*-tetrazol-1-yl)phenyl)isonicotinamide derivatives as novel xanthine oxidase inhibitors, Eur. J. Med. Chem. 183 (2019) 111717. https://doi.org/10.1016/j.ejmech.2019.111717.

[51] M.A. Lill, M.L. Danielson, Computer-aided drug design platform using PyMOL, J. Comput. Aided Mol. Des. 25 (2011) 13-19. https://doi.org/10.1007/s10822-010-9395-8.

Table 1. Antiproliferative activity of target compounds **14a-v** against six human cancer cell lines.

Compounds	R	IC_{50} (μM) [a]					
		A549 [b]	OVCAR-3 [c]	HepG2 [d]	LoVo [e]	PANC-1 [f]	SGC7901 [g]
14a	2-OH	0.23 ± 0.01	0.09 ± 0.01	0.12 ± 0.01	0.54 ± 0.05	0.23 ± 0.02	0.41 ± 0.05
14b	3-OH	0.18 ± 0.01	0.37 ± 0.04	0.07 ± 0.01	0.41 ± 0.08	0.28 ± 0.02	0.27 ± 0.06
14c	4-OH	0.14 ± 0.01	0.41 ± 0.06	0.08 ± 0.01	0.41 ± 0.06	0.10 ± 0.02	0.33 ± 0.17
14d	2-CH_3	0.09 ± 0.04	0.15 ± 0.04	0.15 ± 0.03	0.08 ± 0.01	0.25 ± 0.03	0.35 ± 0.02
14e	3-CH_3	0.05 ± 0.01	0.16 ± 0.01	0.30 ± 0.06	0.05 ± 0.01	0.24 ± 0.02	0.41 ± 0.09
14f	4-CH_3	0.40 ± 0.06	0.04 ± 0.01	0.48 ± 0.06	0.05 ± 0.01	0.27 ± 0.10	0.39 ± 0.05
14g	2-OCH_3	0.35 ± 0.04	0.14 ± 0.03	0.11 ± 0.01	0.07 ± 0.02	0.12 ± 0.01	0.28 ± 0.05
14h	3-OCH_3	0.24 ± 0.04	0.28 ± 0.03	0.07 ± 0.01	0.08 ± 0.01	0.86 ± 0.07	0.59 ± 0.15
14i	4-OCH_3	0.05 ± 0.01	0.25 ± 0.02	0.10 ± 0.01	0.07 ± 0.01	0.33 ± 0.02	0.48 ± 0.08
14j	2-CN	0.10 ± 0.01	0.11 ± 0.01	0.18 ± 0.01	0.14 ± 0.01	0.24 ± 0.01	0.26 ± 0.05
14k	3-CN	0.44 ± 0.08	0.23 ± 0.01	0.04 ± 0.01	0.32 ± 0.03	0.26 ± 0.01	0.25 ± 0.04
14l	4-CN	0.14 ± 0.02	0.38 ± 0.07	0.05 ± 0.01	0.09 ± 0.01	0.25 ± 0.03	0.50 ± 0.23
14m	2-F	0.24 ± 0.01	0.30 ± 0.05	0.06 ± 0.01	0.04 ± 0.01	0.15 ± 0.03	0.30 ± 0.04
14n	3-F	0.18 ± 0.04	0.43 ± 0.06	0.08 ± 0.01	0.09 ± 0.01	0.22 ± 0.08	0.53 ± 0.16
14o	4-F	0.23 ± 0.04	0.20 ± 0.01	0.09 ± 0.02	0.04 ± 0.01	0.11 ± 0.01	0.50 ± 0.19
14p	2-Cl	0.07 ± 0.01	0.04 ± 0.01	0.06 ± 0.01	0.19 ± 0.01	0.27 ± 0.06	0.22 ± 0.09
14q	3-Cl	0.06 ± 0.02	0.05 ± 0.01	0.06 ± 0.02	0.07 ± 0.01	0.26 ± 0.02	0.51 ± 0.14
14r	4-Cl	0.07 ± 0.01	0.16 ± 0.01	0.09 ± 0.02	0.16 ± 0.04	0.44 ± 0.05	0.41 ± 0.01
14s	2-Br	0.13 ± 0.01	0.14 ± 0.03	0.15 ± 0.02	0.06 ± 0.02	0.28 ± 0.05	0.50 ± 0.12
14t	3-Br	**0.09 ± 0.02**	**0.03 ± 0.01**	**0.02 ± 0.01**	**0.03 ± 0.01**	**0.09 ± 0.01**	**0.12 ± 0.02**
14u	4-Br	0.08 ± 0.01	0.14 ± 0.01	0.11 ± 0.02	0.06 ± 0.01	0.20 ± 0.01	0.45 ± 0.06
14v	H	0.07 ± 0.01	0.05 ± 0.02	0.09 ± 0.01	0.05 ± 0.01	0.16 ± 0.01	0.24 ± 0.05
17-AAG	/	> 10	0.48 ± 0.08	0.33 ± 0.04	0.26 ± 0.07	3.21 ± 0.37	> 10

[a] Cells were treated with the indicated compounds for 24 h, and cell viability was determined by MTT methods (IC_{50} = mean ± SD, n = 3). [b] Human lung cancer cell lines, [c] Human ovarian cancer cell lines, [d] Human liver cancer cell lines, [e] Human colon cancer cell lines, [f] Human pancreatic cancer cell lines, [g] Human gastric cancer cell lines.

Table 2. The CC_{50} values of selected compounds **14j**, **14l**, **14m**, **14p**, **14q**, **14t**, **14v** and 17-AAG against six human normal cell lines.

Compounds	CC_{50} (μM) [a]					
	MRC-5 [b]	IOSE80 [c]	LO2 [d]	NCM460 [e]	HPDE6-c7 [f]	GSE-1 [g]
14j	23.33 ± 1.19	13.83 ± 0.43	46.10 ± 1.64	37.49 ± 1.54	16.02 ± 0.83	9.45 ± 0.55
14l	10.75 ± 0.66	5.52 ± 0.17	15.73 ± 0.85	8.14 ± 0.31	> 100	11.25 ± 0.15
14m	15.07 ± 0.96	19.22 ± 0.67	13.27 ± 0.93	5.26 ± 0.92	26.16 ± 0.19	5.16 ± 0.59
14p	4.13 ± 0.81	13.35 ± 0.51	20.12 ± 0.68	10.76 ± 0.78	3.94 ± 0.86	5.37 ± 0.65
14q	8.84 ± 0.89	13.52 ± 0.36	8.51 ± 0.68	8.41 ± 0.62	12.96 ± 0.32	69.83 ± 1.81
14t	**38.84 ± 0.75**	**9.55 ± 0.16**	**10.54 ± 0.34**	**14.56 ± 0.24**	**13.83 ± 0.42**	**9.93 ± 0.76**
14v	9.73 ± 0.46	23.42 ± 1.02	6.23 ± 0.97	19.58 ± 0.95	>100	6.69 ± 0.25
17-AAG	14.24 ± 0.37	21.46 ± 0.22	11.65 ± 0.78	14.21 ± 0.56	19.54 ± 1.05	7.49 ± 0.15

[a] All CC_{50} values (μM) are averages from triplicate assays. (CC_{50} = mean ± SD, n = 3). [b] Human embryo lung fibroblast cell lines, [c] Human normal ovarian epithelial cell lines, [d] Human normal liver cell lines, [e] Human normal colonic epithelial cell lines, [f] Human normal pancreatic ductal epithelial cell lines, [g] Human gastric mucosal cell lines.

Table 3. Hsp90α enzymatic assays of selected compounds **14j**, **14l**, **14m**, **14p**, **14q**, **14t**, **14v** and 17-AAG.

Compounds	IC_{50} (nM) [a]	Compounds	IC_{50} (nM) [a]
14j	7.99 ± 0.74	**14q**	7.38 ± 0.54
14l	21.77 ± 0.53	**14t**	**0.71 ± 0.07**
14m	2.68 ± 0.33	**14v**	34.01 ± 0.93
14p	3.28 ± 0.18	17-AAG	20.21 ± 0.24

[a] All IC_{50} values (nM) are averages from triplicate assays. (IC_{50} = mean ± SD, n = 3).

Figure Caption

Fig. 1. Chemical structures of some Hsp90 inhibitors.

Fig. 2. Design of the compounds **14a-v** by structural simplification and modification.

Fig. 3. Selectivity index of selected compounds **14j**, **14l**, **14m**, **14p**, **14q**, **14t**, **14v** and 17-AAG.

Fig. 4. The docking pose of compound **14t** (green sticks) in the ATP-binding pocket of human Hsp90α (PDB ID: 2XJX). Binding interactions are showed as dashed lines: hydrogen bond (green), hydrophobic interaction (grey) and halogen bond (purple). The docking poses were visualized using PyMOL.

Fig. 5. Compound **14t** induced cell cycle arrest in LoVo and SW620 cells**.** Effects of compound **14t** on cell cycle were evidenced by PI staining and flow cytometry analysis. Each column represented the mean ± SD of triplicate determinations (where *P < 0.05, **P < 0.01 and ***P < 0.001 compared to control).

Fig. 6. Compound **14t** induced apoptosis in LoVo and SW620 cells. Effects of **14t** on cell death were evidenced by Annexin V-FITC/PI staining and flow cytometry analysis. Apoptotic cells were Annexin V [+] and PI [−], late apoptotic cells were Annexin V [+] and PI [+], necrotic cells were Annexin V [−] and PI [+] and living cells were Annexin V [−] and PI [−]. Each column represented the mean ± SD of triplicate determinations (where *P < 0.05, **P < 0.01 and ***P < 0.001 compared to control).

Fig. 7. Effects of compound **14t** on the apoptotic protein expression in LoVo and SW620 cells. Cells were treated with compound **14t** for 24 h; then, the total proteins were extracted and subjected to western blot analysis using antibodies against bax, bcl-2, cleaved-caspase 3 and caspase 3, β-actin was used as an internal control. Relative protein expression of bax/bcl-2 and cleaved-caspase 3/caspase 3 in LoVo and SW620 cells were calculated. Each column represented the mean ± SD of triplicate determinations (where *P < 0.05, **P < 0.01 and ***P < 0.001 compared to control).

Fig. 8. Effects of compound **14t** on LoVo and SW620 cells migration. For transwell assay, the migrated cells on

the lower surface of the membrane were quantified by counting the number of cells in ten random fields per membrane and expressed as cells/fields. The scale bars indicate 100 μm. For wound healing assay, the red line is the cell migration edge, and cell healing rates were calculated by the fraction of cell coverage across the line. Each column represented the mean ± SD of triplicate determinations (where *P < 0.05, **P < 0.01 and ***P < 0.001 compared to control).

Fig. 9. Inhibitory effects of **14t** on the growth of SW620 tumors *in vivo*. Mice inoculated with SW620 tumors were intraperitoneally treated with 17-AAG or **14t**. (A) The weights of mice were measured at the indicated time points. (B) The volumes of tumors were measured at the indicated time points. (C) Representative images of the tumors from each group were captured. (D) The tumor growth inhibition (TGI) values of 17-AAG and **14t**. (E) Ki67 and cleaved-caspase 3 immunohistochemical staining of tumors. Data are shown as mean ± SD from each group of mice, n= 5. Where *P < 0.05, **P < 0.01 and ***P < 0.001 compared to control.

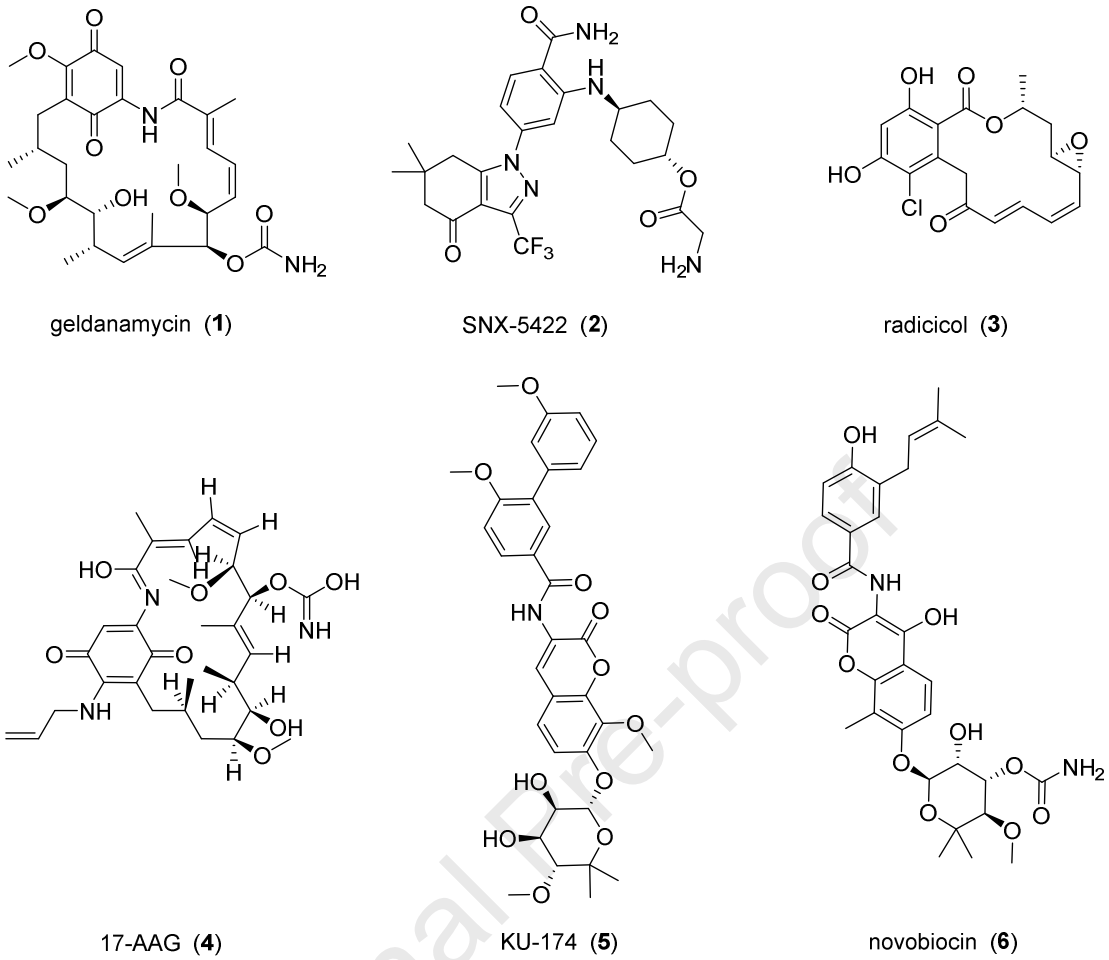

Fig. 1. Chemical structures of some Hsp90 inhibitors.

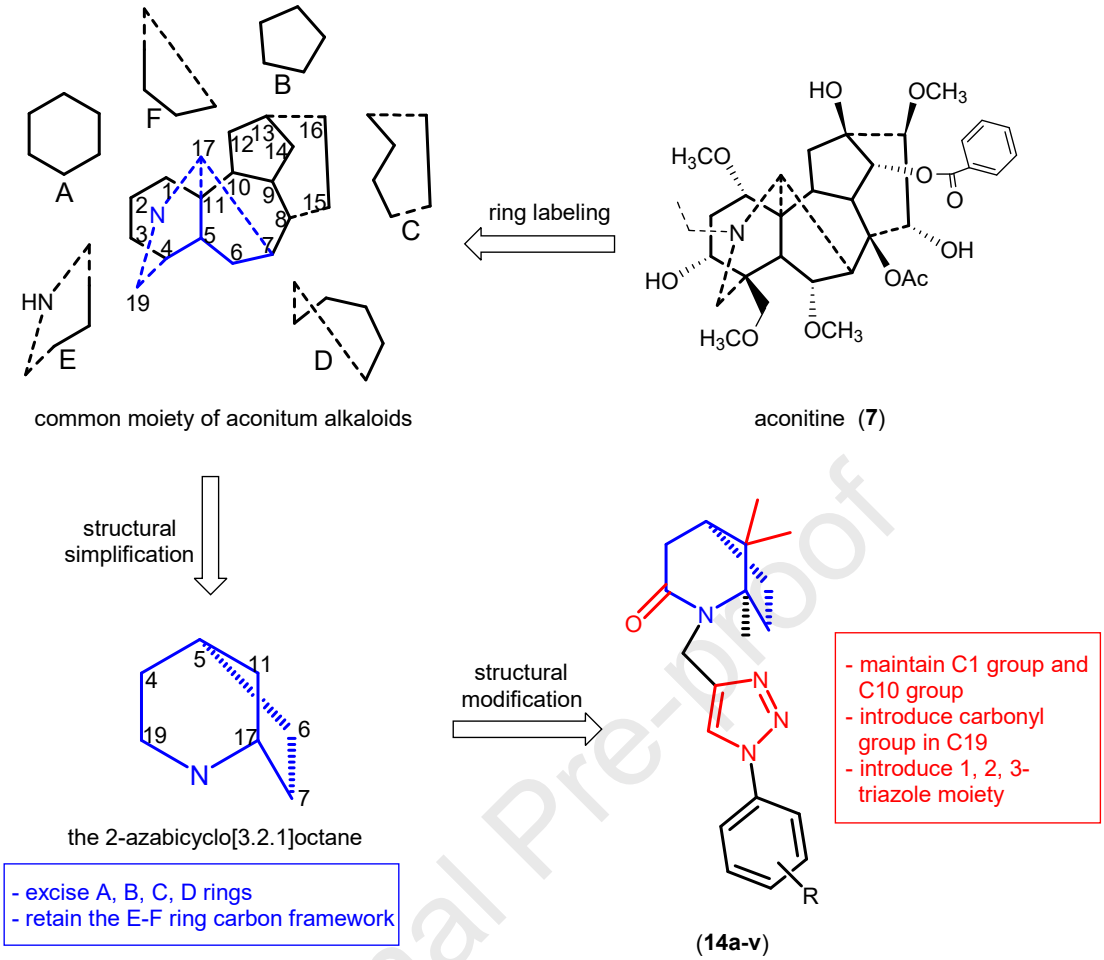

Fig. 2. Design of the compounds **14a-v** by structural simplification and modification.

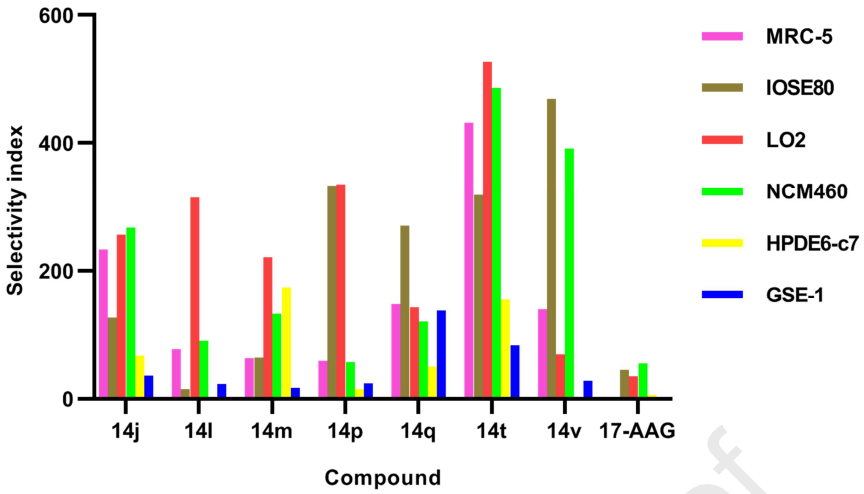

Fig. 3. Selectivity index of selected compounds **14j**, **14l**, **14m**, **14p**, **14q**, **14t**, **14v** and 17-AAG.

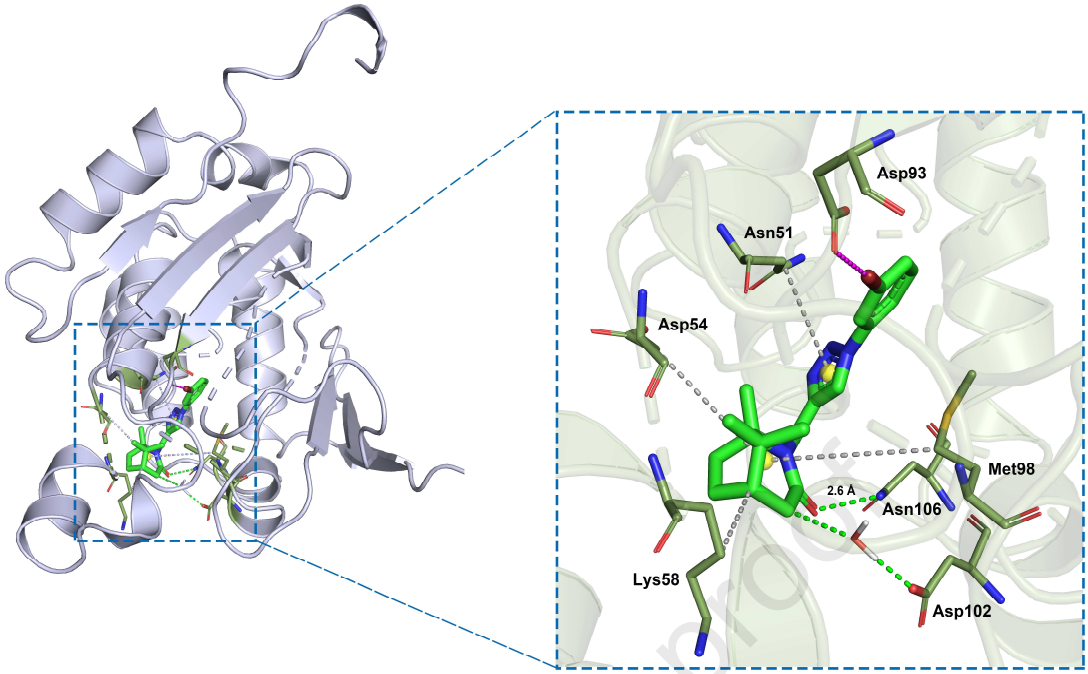

Fig. 4. The docking pose of compound **14t** (green sticks) in the ATP-binding pocket of human Hsp90α (PDB ID: 2XJX). Binding interactions are showed as dashed lines: hydrogen bond (green), hydrophobic interaction (grey) and halogen bond (purple). The docking poses were visualized using PyMOL.

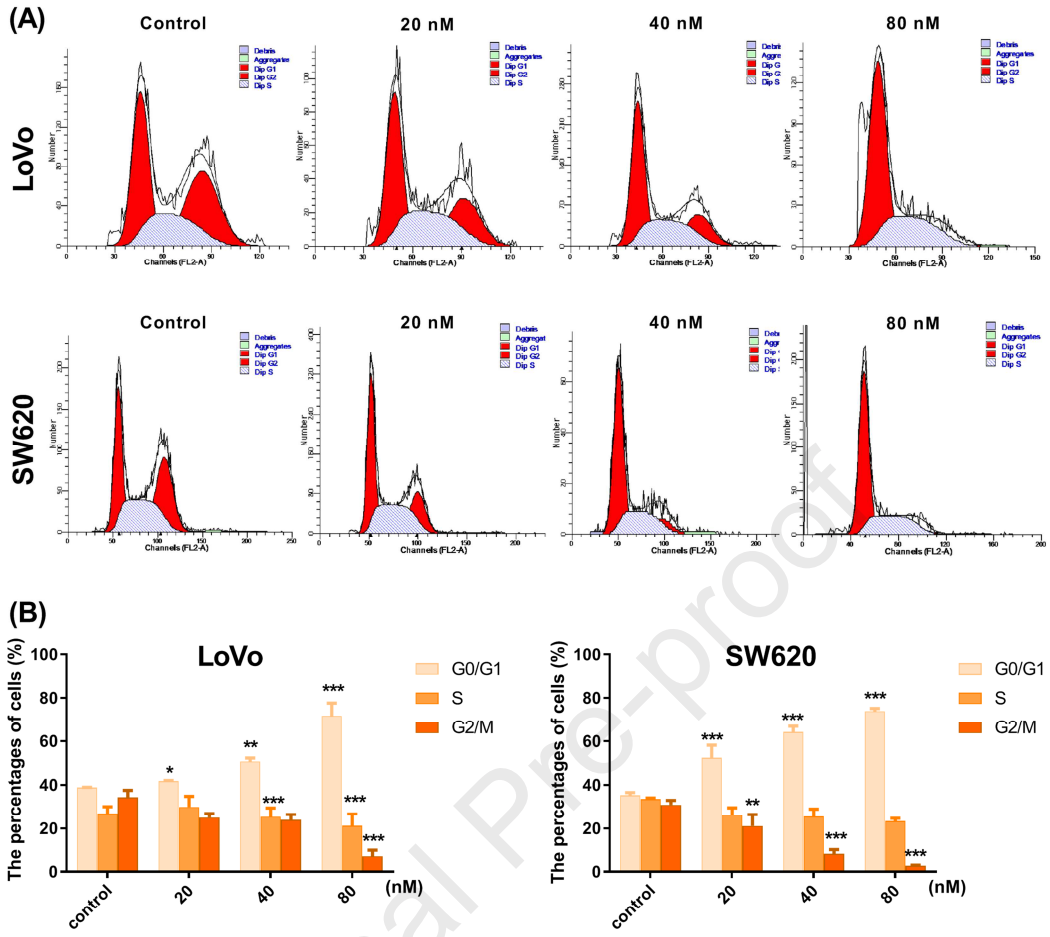

Fig. 5. Compound **14t** induced cell cycle arrest in LoVo and SW620 cells**.** Effects of compound **14t** on cell cycle were evidenced by PI staining and flow cytometry analysis. Each column represented the mean ± SD of triplicate determinations (where *P < 0.05, **P < 0.01 and ***P < 0.001 compared to control).

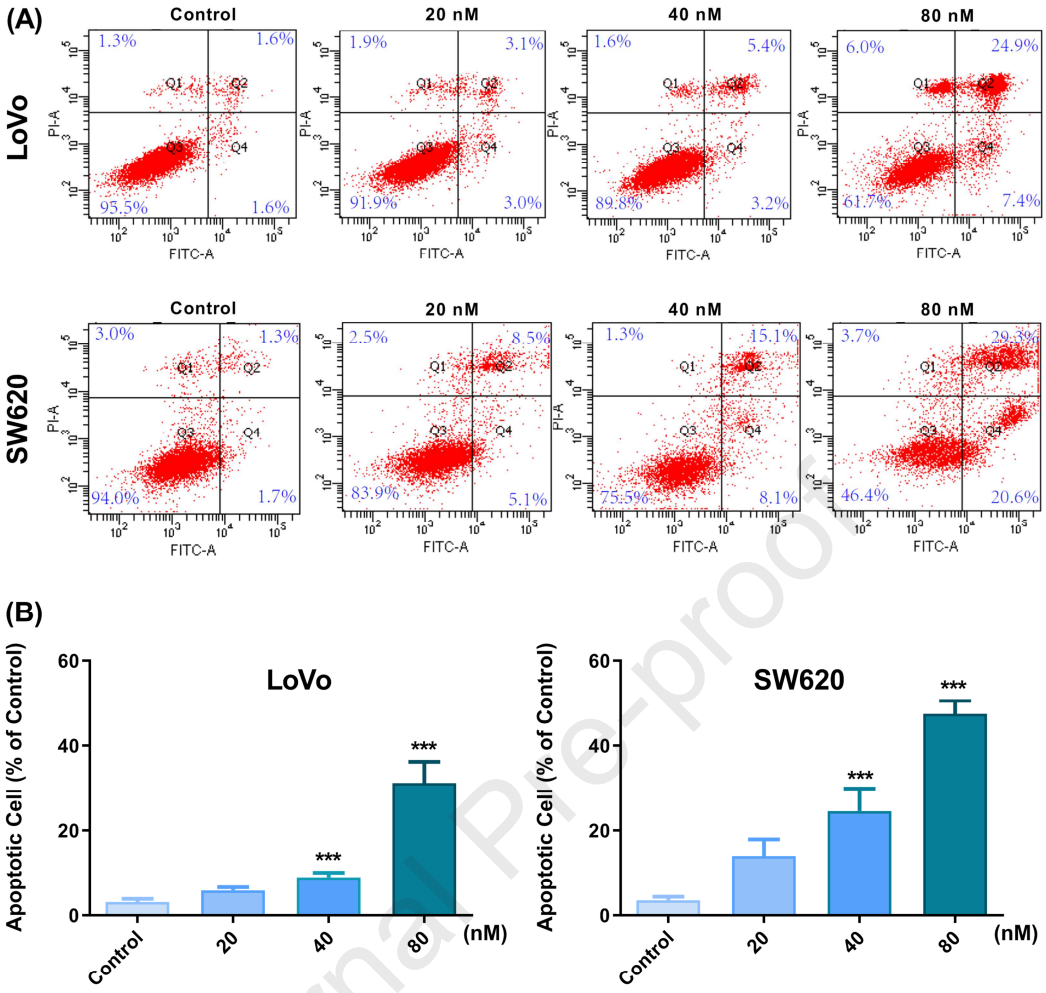

Fig. 6. Compound **14t** induced apoptosis in LoVo and SW620 cells. Effects of **14t** on cell death were evidenced by Annexin V-FITC/PI staining and flow cytometry analysis. Apoptotic cells were Annexin V [+] and PI [−], late apoptotic cells were Annexin V [+] and PI [+], necrotic cells were Annexin V [−] and PI [+] and living cells were Annexin V [−] and PI [−]. Each column represented the mean ± SD of triplicate determinations (where *P < 0.05, **P < 0.01 and ***P < 0.001 compared to control).

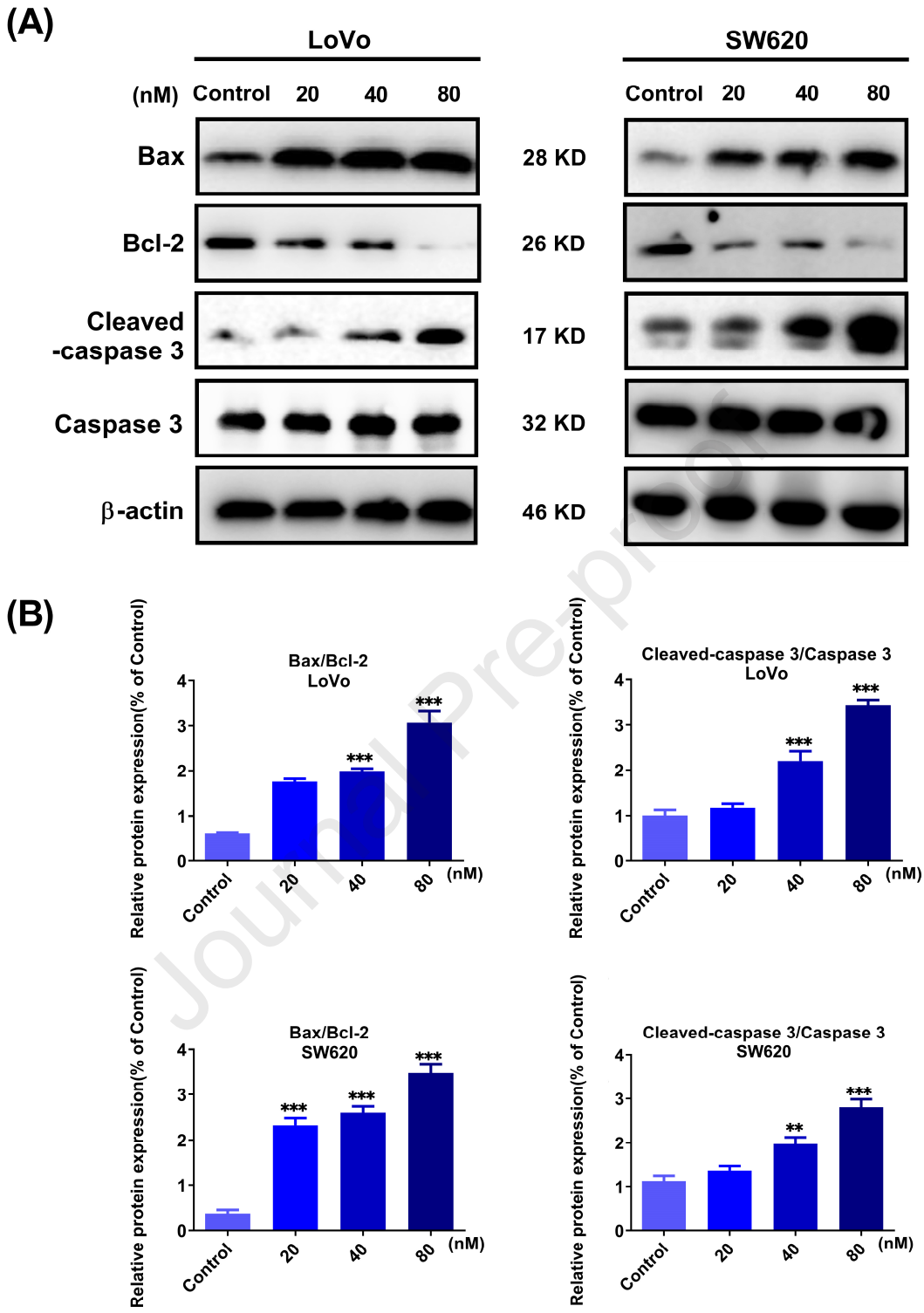

Fig. 7. Effects of compound **14t** on the apoptotic protein expression in LoVo and SW620 cells. Cells were treated with compound **14t** for 24 h; then, the total proteins were extracted and subjected to western blot analysis using antibodies against bax, bcl-2, cleaved-caspase 3 and caspase 3, β-actin was used as an internal control. Relative protein expression of bax/bcl-2 and cleaved-caspase 3/caspase 3 in LoVo and SW620 cells were calculated. Each column represented the mean ± SD of triplicate determinations (where *P < 0.05, **P < 0.01 and ***P < 0.001 compared to control).

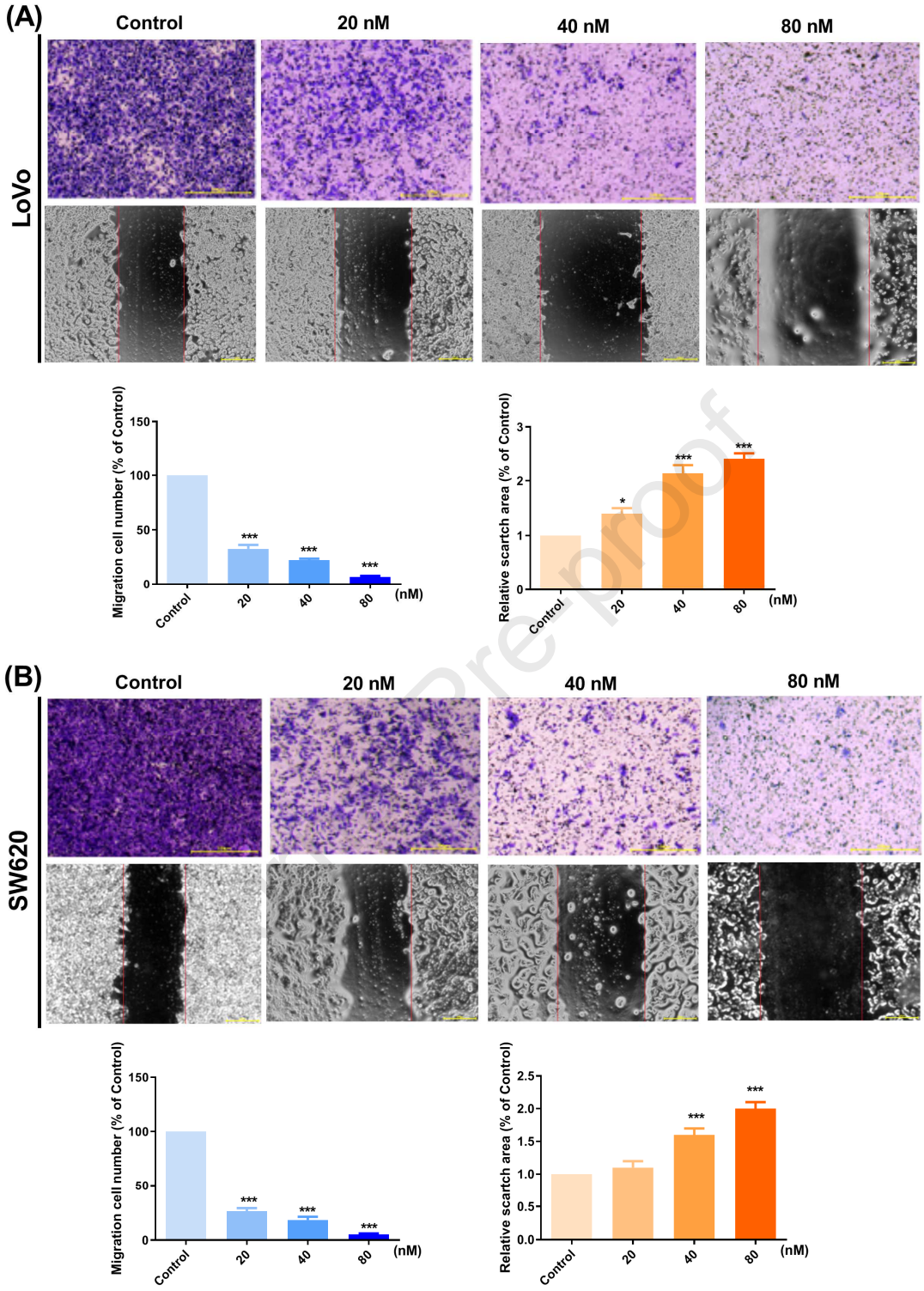

Fig. 8. Effects of compound **14t** on LoVo and SW620 cells migration. For transwell assay, the migrated cells on the lower surface of the membrane were quantified by counting the number of cells in ten random fields per membrane and expressed as cells/fields. The scale bars indicate 100 μm. For wound healing assay, the red line is the cell migration edge, and cell healing rates were calculated by the fraction of cell coverage across the line. Each column represented the mean ± SD of triplicate determinations (where *P < 0.05, **P < 0.01 and ***P < 0.001 compared to control).

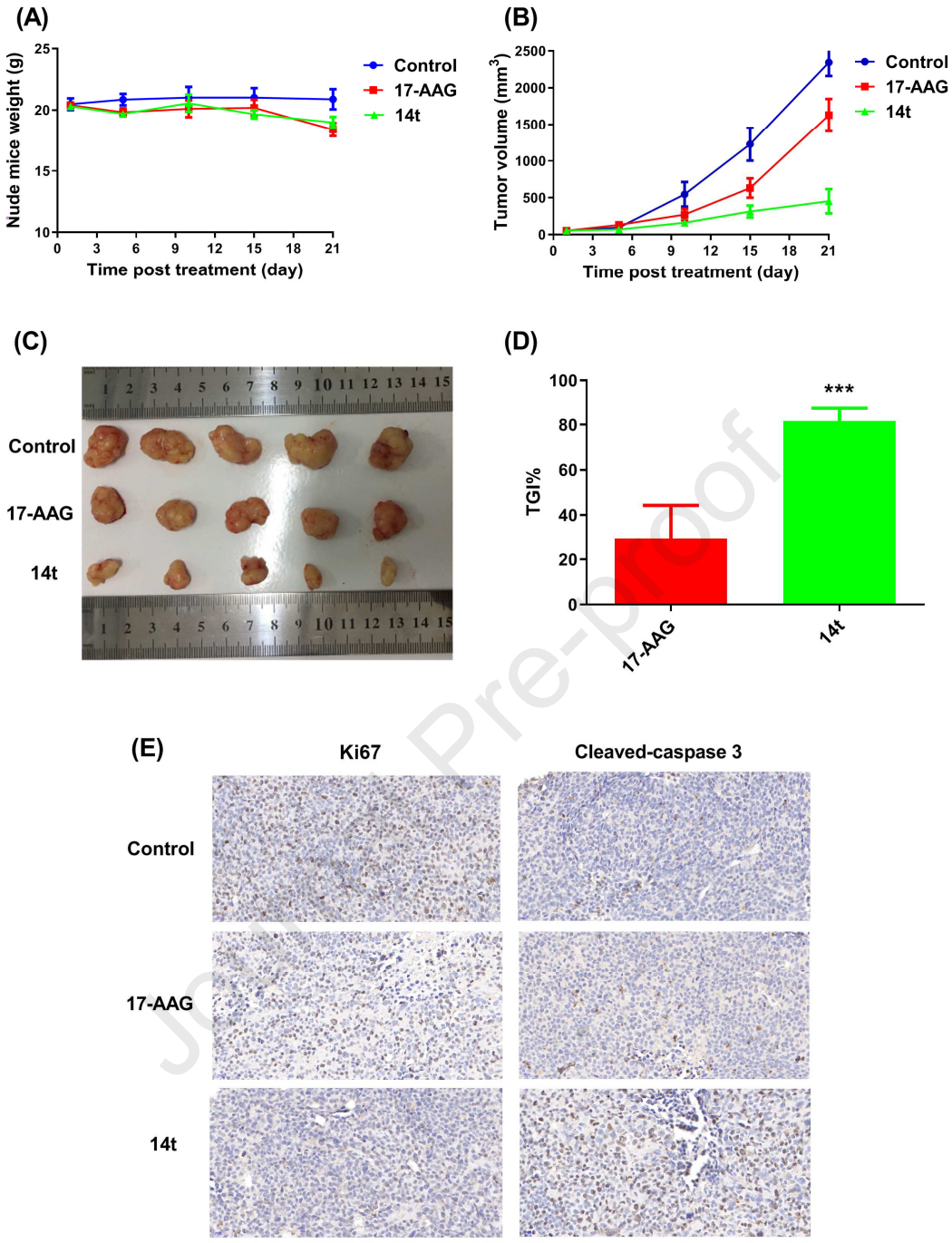

Fig. 9. Inhibitory effects of **14t** on the growth of SW620 tumors *in vivo*. Mice inoculated with SW620 tumors were intraperitoneally treated with 17-AAG or **14t**. (A) The weights of mice were measured at the indicated time points. (B) The volumes of tumors were measured at the indicated time points. (C) Representative images of the tumors from each group were captured. (D) The tumor growth inhibition (TGI) values of 17-AAG and **14t**. (E) Ki67 and cleaved-caspase 3 immunohistochemical staining of tumors. Data are shown as mean ± SD from each group of mice, n= 5. Where *P < 0.05, **P < 0.01 and ***P < 0.001 compared to control.

Scheme 1

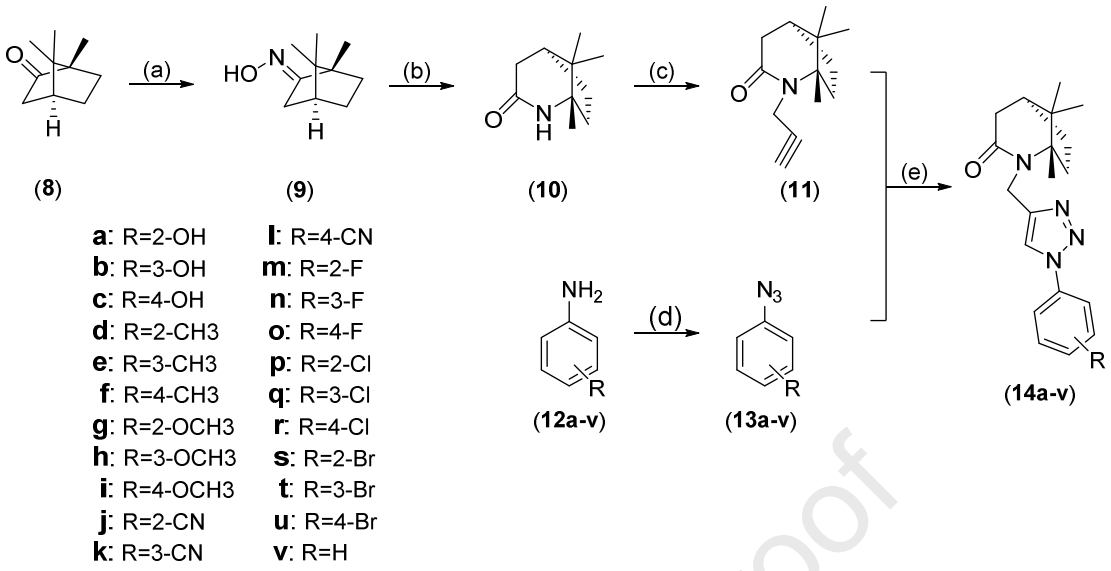

Scheme 1. Reagents and conditions: (a) AcONa, H_2NOH•HCl, MeOH, H_2O, 80 °C, 9 h; (b) $MeSO_2Cl$, pyridine, −22 °C, 3 h to rt, 2 h; (c) NaH, propargyl bromide, THF, 0 °C, 1 h to rt, 5 h; (d) $NaNO_2$, HCl, NaN_3, CH_2Cl_2, H_2O, 0 °C, 1 h to rt, 3-5 h; (e) $CuSO_4$•$5H_2O$, ascorbic acid, t-BuOH, H_2O, 60 °C, 8 h.

Highlights:

- A series of 2-azabicyclo [3.2.1] octane derivatives was designed and synthesized.
- Antitumor activities of these compounds were evaluated in six cancer cell lines.
- Compound **14t** induced G1/S cell cycle arrest and apoptosis in LoVo and SW620 cells.
- Compound **14t** significantly reduced the volumes and size of colon tumors in mice.

Declaration of interests

☒ The authors declare that they have no known competing financial interests or personal relationships that could have appeared to influence the work reported in this paper.

☐The authors declare the following financial interests/personal relationships which may be considered as potential competing interests: